Energy & Environmental Science

REVIEW

New developments in composites, copolymer technologies and processing techniques for flexible fluoropolymer piezoelectric generators for efficient energy harvesting

Received 12th October 2018,
Accepted 25th January 2019

DOI: 10.1039/c8ee03006e

rsc.li/ees

Nick Adamson,[a] Alexey M. Glushenkov,[a] Vanessa C. Lussini,[b] Phillip J. Fox,[b] Greg W. Dicinoski, [b] Joseph G. Shapter [c] and Amanda V. Ellis *[a]

Flexible piezoelectric generators (PEGs) have recently attracted significant interest, as they are able to harvest mechanical energy and convert it to electricity, decreasing reliance on conventional energy sources. These devices enable innovative applications including smart clothing, wearable electronics, on-skin and implantable sensors, as well as harvesting energy from the movement of vehicles, water and wind. Poly(vinylidene fluoride) and related fluoropolymers are the most common flexible piezoelectric materials, widely utilized for their high electromechanical conversion efficiencies, optimal mechanical flexibility, processability and biocompatibility. This critical review covers the processing of fluoropolymers towards the maximization of piezoelectric conversion parameters. Particular emphasis is placed on the correlation between synthetic routes, inclusion of further co-monomers, addition of additives and nanomaterials, as well as processing techniques and the optimized electricity generation in the resultant PEGs, providing an important analysis to complement existing literature. The importance of novel polymer deposition techniques, which reduce reliance on the conventional, highly energetic post-processing steps, are highlighted. Recent advances in fluoropolymer-based flexible PEGs open an array of exciting applications, which rapidly progress towards commercialization. This review provides a timely analysis of this increasingly important field to the cross-disciplinary community of polymer chemists, materials scientists, nanotechnologists, engineers, and industry practitioners.

1. Introduction

Harvesting energy into a usable form through sustainable methods is gaining importance for portable and wearable electronics and sensors. According to the requirements of portable electronic devices and in-line with the trend of miniaturization of wearable electronics, conversion of energy to electricity from a number of sources is possible.[1, 2] Sustainable electrical generators have been proposed which utilize solar, thermal and mechanical energies. Photovoltaic generators produce useable energy from sunlight, with experimental power conversion efficiencies up to 13% in flexible and organic solar cells; however, they are limited to daytime operation for conversion and require large areas continuously exposed to direct sunlight.[3, 4] Commercialization of photovoltaics as electrical generators has occurred, and solar cells are currently regarded as the most prominent source of small-scale sustainable energy in industry.[5]

Pyroelectric generators that harvest electricity from changes in temperature have been proposed. The power efficiency of these devices is typically below 3% at temperatures near 25 °C and they possess a slow electrical output response.[6] The advantage of these types of harvesters is that they can be used in environments where significant and frequent temperature changes occur. Bowen *et al*.[7] provide a recent in-depth review of pyroelectric generators.

Scavenging mechanical energy through piezoelectricity is a prospective solution due to high energy conversion efficiencies up to 75% in inorganic materials and 37% in fluoropolymers.[8-11] These systems are broadly referred to as piezoelectric generators (PEGs) and are the topic of this review.

Piezoelectricity occurs in crystalline dielectric materials possessing a dipole moment. The concept of electromechanical coupling through piezoelectricity has been proposed and experimentally verified in the nineteenth century by Curie *et al*.[12, 13] and Lippmann[14]. During the first half of the twentieth century, piezoelectric materials have found limited industrial uses in sensors and actuators.[15-17] However, in 1961 Sonus Corporation patented the first energy harvesters using PEGs .[18] The electric output from the induced strain through stretching, bending or compression of piezoelectric materials has been shown to power electrical items, such as light emitting diodes (LEDs), liquid crystal displays (LCDs), MP3 players, and sensors.[19-24] This ability to generate electricity through the use

[a] Department of Chemical Engineering, The University of Melbourne, Parkville, Victoria 3010, Australia. E-mail: amanda.ellis@unimelb.edu.au
[b] Note Issue Department, Reserve Bank of Australia, Craigieburn, Victoria 3062, Australia.
[c] Australian Institute of Bioengineering and Nanotechnology, The University of Queensland, Brisbane, Queensland 4072, Australia

of PEGs has the potential to supplement the use of batteries or remove them in some applications where only intermittent power is required.

Piezoelectric materials span from naturally-found crystals to synthetic ceramics, polymers and nanostructured metal oxides.[25] Early literature has focused solely on the transduction mechanism in quartz, Rochelle salt, and other naturally-occurring anisotropic crystals.[12, 26]

The ability to fabricate advanced inorganic structures led to the development of perovskites showing enhanced piezoelectricity due to the polarization of the central atom within the unit cell.[27, 28] A class of synthetic polymers with a dipole moment perpendicular to the backbone have since gained attention as flexible piezoelectric materials, enabling the utilization of flexible and biocompatible PEGs in wearable electronics and *in-vivo* sensors.[29, 30] Recent advances have incorporated into these polymers nanostructured perovskites and inorganic oxides in the form of nanoparticles and nanowires. The incorporation of these nanofillers has shown promise in increasing the electrical output of flexible PEGs.[31-35]

Polymers, in comparison to ceramic materials, tend to exhibit a variety of properties beneficial for uses as PEGs. The 2014 review by Ramadan *et al*.[11] has comparatively analyzed the benefits of piezoelectric polymers and their composites relative to common inorganic materials, suggesting their enhanced mechanical flexibility, lower costs and increased ease of production, as well as biocompatibility for uses such as implantable or wearable sensors. Through tailored processing parameters, piezoelectric polymers have shown high optical transparency and low haze, leading to potential applications in capacitive touch sensors as a top layer on LED displays.[36-38] Recent utilization of nanomaterials and fillers has been reported to increase electromechanical coupling efficiencies of piezoelectric polymers, with the potential of retaining optical transparency, leading to highly efficient flexible and transparent PEGs.[39, 40]

Poly(vinylidene fluoride) (PVDF) and related fluoropolymers are the most common commercialized piezoelectric polymers.[41, 42] These polymers are stable at room temperature, simple to process using conventional solvent casting and melt-extrusion techniques, chemically inert, biocompatible and exhibit conversion efficiencies higher than those of other piezoelectric polymers.[11, 43] These properties make fluoropolymers ideal for use as sustainable electrical generators for powering portable, wearable and implantable sensors and electrical devices, with or without an integrated energy storage solution.

This review is focused on the factors influencing the electrical output in flexible piezoelectric PVDF-based fluoropolymers and how these factors can be controlled to maximize energy conversion, providing a critical analysis of the recent literature on polymerization and processing techniques and parameters, as well as device geometries. The theory of piezoelectricity in materials and the operating principles of PEGs are introduced first. The synthesis of PVDF and related fluoropolymers is subsequently discussed with reference to literature and a special focus on decreasing defects, increasing the electroactive phase fractions and the optimization of electromechanical conversion efficiencies. The latest developments in processing of fluoropolymers, such as 3D printing and electrospinning, are reviewed next, and their potential in manufacturing PEGs is discussed and compared to conventional techniques including solvent casting, melt extrusion, and melt-drawing. The inclusion of nanofillers and additives into the polymers is presented as a preferred single-step method to reorient polymer chains, superior to conventional, high-energy multi-step processes. This review highlights the on-going evolution of the field and aims to identify future directions towards the development of commercially relevant low-energy processing methods to produce PVDF-based PEGs.

2. Metrics and definitions for piezoelectric materials

Let us first look at the phenomena in piezoelectric materials and the mathematical toolkit used to describe them. Unlike non-piezoelectric dielectrics, a net dipole moment is present in piezoelectric materials in the absence of external stimuli. When a force is applied, an instantaneous electric field is generated parallel to the direction of the polarization vector. This electric field is proportional to the time-differential of strain and leads to separation of positive and negative surface charges on the opposite surfaces of the material, with a fast response time. When an external load is connected to electrodes deposited on the opposing surfaces, the surface charges force electron migration across the load to neutralize the potential difference between the electrodes. The behavior of piezoelectric materials and the aforementioned transient phenomena are described by directional coefficients and a number of mathematical equations. We will now proceed to the discussion of the mathematical foundation of piezoelectricity in materials.

It is widely accepted that all linear elastic materials exhibit a displacement (x) with applied force (F), related by a spring constant (k). This relationship is known as Hooke's law.[44, 45] This equation is given for the simplest one-dimensional scenario in Eqn (1).

$$F = kx \tag{1}$$

Strain (S) and stress (T) are related by a similar equation with elastic compliance (s) as a proportionality coefficient. In the simplest, one-dimensional case, Eqn (2) applies.

$$S = sT \tag{2}$$

Furthermore, dielectric elastic materials are polarizable when placed under an external electric field. The constitutive equation for such materials is given in Eqn (3).

$$D = \varepsilon E \tag{3}$$

In this equation, the electric displacement (*D*) depends on the permittivity (ε) of the material and the applied electric field (*E*). In piezoelectric materials, the properties described in Eqns (2) and (3) are interrelated and the following Eqns (4) and (5) can be written in a one-dimensional situation.

$$S = s^E T + d^t E \quad (4)$$

$$D = dT + \varepsilon^T E \quad (5)$$

Here, the relationship coefficient (*d*) is termed as the piezoelectric charge coefficient, d^t is the piezoelectric charge coefficient for the case of the inverse piezoelectric effect, and superscripts *E* and *T* refer to constant electric field and stress, respectively.

In reality, to describe piezoelectric phenomena, one should consider the descriptions of the processes in three dimensions. In particular, the requirement for piezoelectricity is a net dipole moment oriented along one direction of the material in question. To aid understanding, the directionality used in defining piezoelectric properties is shown in Fig. 1. Note that rotational directions 4, 5, and 6 are also introduced when directionality is considered in three dimensions. For the clarity of presentation, let us assume that this direction coincides with the z axis (Fig. 1 direction 3). In such a case, piezoelectric properties in x (1) and y (2) directions (Fig. 1 directions 1 and 2) can be considered identical and that of the 3 direction is non-equivalent relative to the others. Taking into account the anisotropy of piezoelectric materials, Eqns (4) and (5) take on the form shown in Eqns (6) and (7), where the constituents are replaced with their tensor analogues.

$$S_p = s^E_{pq} T_q + d_{ip} E_i \quad (6)$$

$$D_i = d_{iq} T_q + \varepsilon^T_{ik} E_k \quad (7)$$

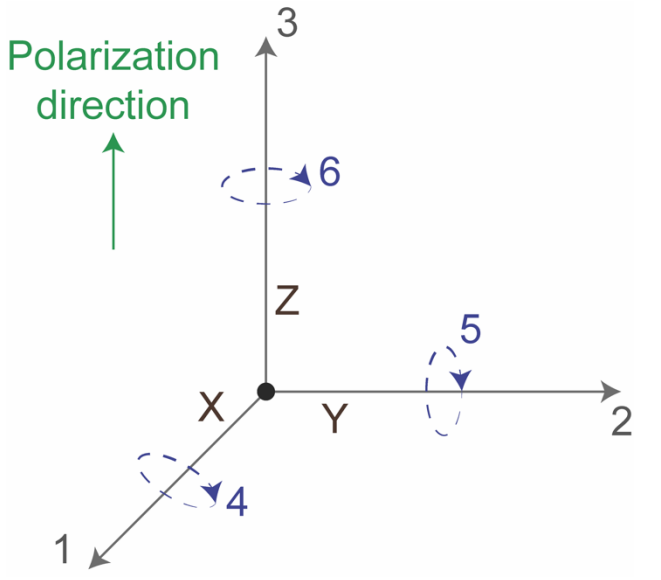

Figure 1: Schematic of reference directions for piezoelectric materials.

In this form, subscripts *i* and *k* represent directions 1, 2 or 3, and *p* and *q* represent directions 1, 2, 3, 4, 5 or 6. When expanded, the equations form a matrix relating strain, stress, electric displacement and electric field, as shown in Eqn (8).

$$\begin{pmatrix} S_1 \\ S_2 \\ S_3 \\ S_4 \\ S_5 \\ S_6 \\ D_1 \\ D_2 \\ D_3 \end{pmatrix} = \begin{pmatrix} S_{11} \\ S_{22} \\ S_{33} \\ 2S_{23} \\ 2S_{13} \\ 2S_{12} \\ D_1 \\ D_2 \\ D_3 \end{pmatrix} = \begin{pmatrix} s^E_{11} & s^E_{12} & s^E_{13} & 0 & 0 & 0 & 0 & 0 & d_{31} \\ s^E_{21} & s^E_{22} & s^E_{23} & 0 & 0 & 0 & 0 & 0 & d_{32} \\ s^E_{31} & s^E_{32} & s^E_{33} & 0 & 0 & 0 & 0 & 0 & d_{33} \\ 0 & 0 & 0 & s^E_{44} & 0 & 0 & 0 & d_{24} & 0 \\ 0 & 0 & 0 & 0 & s^E_{55} & 0 & d_{15} & 0 & 0 \\ 0 & 0 & 0 & 0 & 0 & s^E_{66} & 0 & 0 & 0 \\ 0 & 0 & 0 & 0 & d_{15} & 0 & \varepsilon^T_{11} & 0 & 0 \\ 0 & 0 & 0 & d_{24} & 0 & 0 & 0 & \varepsilon^T_{22} & 0 \\ d_{31} & d_{32} & d_{33} & 0 & 0 & 0 & 0 & 0 & \varepsilon^T_{33} \end{pmatrix} \begin{pmatrix} T_1 \\ T_2 \\ T_3 \\ T_4 \\ T_5 \\ T_6 \\ E_1 \\ E_2 \\ E_3 \end{pmatrix} \quad (8)$$

Here, the values for *p* and *q* are used to simplify indices according to the following rules: 1⇒11, 2⇒22, 3⇒33, 4⇒23≡32, 5⇒13≡31 and 6⇒12≡21.[46-48] One of the alternate forms of the constitutive equations is given using the piezoelectric voltage coefficient (*g*) (as opposed to the piezoelectric charge coefficient), shown in Eqns (9) and (10).

$$S_p = s^D_{pq} T_q + g_{ip} D_i \quad (9)$$

$$E_i = -g_{iq} T_q + \beta^T_{ik} D_k \quad (10)$$

Here, the mechanical compliance (s^D) at constant electric displacement is related to s^E by $s^D = s^E - d^2/\varepsilon^T$ and the impermittivity at constant stress (β^T) is the inverse of ε^T. Furthermore, it should be noted that *g* and *d* are related via $g = d/\varepsilon^T$.[47]

The equations for displacement current (J_D), open circuit voltage (V_{OC}) and current transport were discussed in a recent review by Wang[49] based on Ampere's circuital law with Maxwell's addition. The displacement current as postulated by Maxwell is shown in Eqn (11), formulated to supplement Ampere's law for magnetic fields with regards to contribution from electric charges. This equation is a differential form of Equation 3 for dielectric materials with respect to time.

$$J_D = \frac{\partial D}{\partial t} = \varepsilon \frac{\partial E}{\partial T} + \frac{\partial P}{\partial t} \quad (11)$$

The displacement current is noted to be a time-dependent electric field for either vacuum (utilizing $\varepsilon = \varepsilon_0$, the permittivity of vacuum) or alternate media such as a dielectric material, rather than the conventional definition of current utilizing the movement of charges. The reason for this distinction arises from the second term in Eqn (11), the time-dependent dielectric polarization within the material ($\partial P/\partial t$). Since $P_i = d_{iq}T_q$ (rearranged from Eqn (7)), the displacement current arising from polarization of the material is shown in Eqn (12).

$$J_D = \frac{\partial P_i}{\partial t} = d_{iq}\left(\frac{\partial T}{\partial t}\right)_q = h_{iq}\left(\frac{\partial S}{\partial t}\right)_q \quad (12)$$

Here, the piezoelectric coefficient is $h_{iq} = d_{iq}/(s^E_{pq}\varepsilon^T_{ik})$. Eqn (12) suggests that the output arises from a time-dependent variation of strain, proportional to a time-dependent variation of the polarization vector. Furthermore, the equations for V_{OC} and the current transport for piezoelectric materials with electrodes attached across the thickness axis are given in Eqns (13) and (14), respectively.

$$V_{OC} = \frac{l_3\sigma_m(l_3)}{\varepsilon_{33}} \quad (13)$$

$$RA\left(\frac{d\sigma}{dt}\right) = \frac{l_3(\sigma_m(l_3)-\sigma_e(l_3))}{\varepsilon_{33}} \quad (14)$$

Here, l_3 represents thickness of the piezoelectric material (also the distance between electrodes), ε_{33} represents permittivity of the piezoelectric material, $\sigma_m(l_3)$ is the density of piezoelectric charges on the surface of the material, $\sigma_e(l_3)$ is the charge density of mobile electrons within the electrodes, A is the surface area of electrodes and R is the resistance of the attached external load. Eqn (13) suggests a direct relationship between V_{OC} and thickness, as well as an inverse relationship with the dielectric constant—implying a material with lower ε_{33} such as a fluoropolymer can exhibit higher open circuit voltage relative to ceramic materials. Furthermore, Equation 14 implies dependence of the time-dependent current transport on the load resistance and electrode properties.

The transport phenomena in Eqns (12), (13) and (14) explain the operational principles in PEGs, whereby factors such as strain, time-dependent strain rate, directionality of strain, thickness of material, dipolar strength, anisotropic dielectric permittivity of the piezoelectric material, quality and surface area of the electrode can all play a role in the development of efficient PEGs.

For the indiscriminate comparative analysis of piezoelectric materials used in PEGs, a figure of merit (FOM) is required. For a long time, the electromechanical coupling coefficient k^2 has been considered as the non-biased FOM, as shown for the 33 directionality in Eqn (15).[50]

$$k^2_{33} = \frac{stored\ electrical\ energy}{input\ mechanical\ energy} = \frac{d^2_{33}}{s^E_{33}\varepsilon^T_{33}} \quad (15)$$

The relationship between the piezoelectric charge (d) and voltage (g) coefficients, as shown above, is $d_{33} = g_{33} / \varepsilon^T_{33}$, allowing Eqn (15) to be expressed as a function of both coefficients. Furthermore, the Young's modulus of a material, defined as the ratio of stress and strain (T/S) from Eqn (2), is inversely proportional to the mechanical compliance at constant electric field (s^E). Hence, the coupling coefficient relationship from Eqn (15) then takes on the form shown in Eqn (16).

$$k^2_{33} = d_{33}g_{33}Y_3 \quad (16)$$

Recently, Deutz *et al*.[51] have investigated the FOM for a variety of piezoelectric materials, suggesting that the k^2 value does not consistently represent the stored electrical energy per unit volume (U_{open}) in the sample. They have proposed that U_{open} scales linearly with the product of the charge and the voltage coefficients, shown in Eqn (17) and Fig. 2.

$$U_{open} = \frac{1}{2}d_{33}g_{33}\left(\frac{\Delta F}{A_e}\right)^2 \quad (17)$$

Here, the ΔF denotes the input force amplitude and A_e stands for the electrode area. This research has verified the proposed model using a purpose-built electrometer (Fig. 2a,b) and measuring U_{open} as a function of $d_{33}g_{33}$ (Fig. 2c) for a range of piezoelectric materials including perovskites, fluoropolymers and perovskite-polymer composites. The study has shown good agreement for varying materials (Fig. 2c-e), varying $g_{33}d_{33}$ (Fig. 2c) and varying applied force (Fig. 2d). The relationship in Eqn (17) has been argued to describe the electromechanical conversion in all piezoelectric materials irrespective of their composition, morphology or geometry. It is also noted to be independent of the elastic compliance, unlike the equation for the k^2 coefficient. In previous literature, the piezoelectric ceramics have been reported with significantly higher k^2 relative to flexible polymeric materials. The use of $d_{33}g_{33}$ as an unbiased FOM suggests that flexible materials are highly effective in their use as PEGs.

3. Properties of poly(vinylidene fluoride) (PVDF)

Among the variety of materials exhibiting piezoelectricity, polymers are of interest due to several enhanced properties desirable in flexible PEGs, such as the ability to deform, ease of processing and low dielectric constant. In particular, polymers possessing a dipole moment perpendicular to the backbone have been found to exhibit piezoelectric properties.[52] This phenomenon is particularly evident in fluorinated polymers such as PVDF, whereby two fluorine atoms are attached to every second carbon atom along a vinyl backbone (Fig. 3(a-c)). If the fluorine atoms are arranged a certain way, the chain substituents orient in a manner that shows an effective dipole perpendicular to the chain.[9] This is described further in the following section. PVDF and its co-polymers remain the most interesting and widely researched polymeric materials for flexible PEGs.

3.1. β phase as the preferred structural orientation and its electromechanical coupling properties

The properties of PVDF are influenced directly by its structure. It is a semi-crystalline polymer with properties

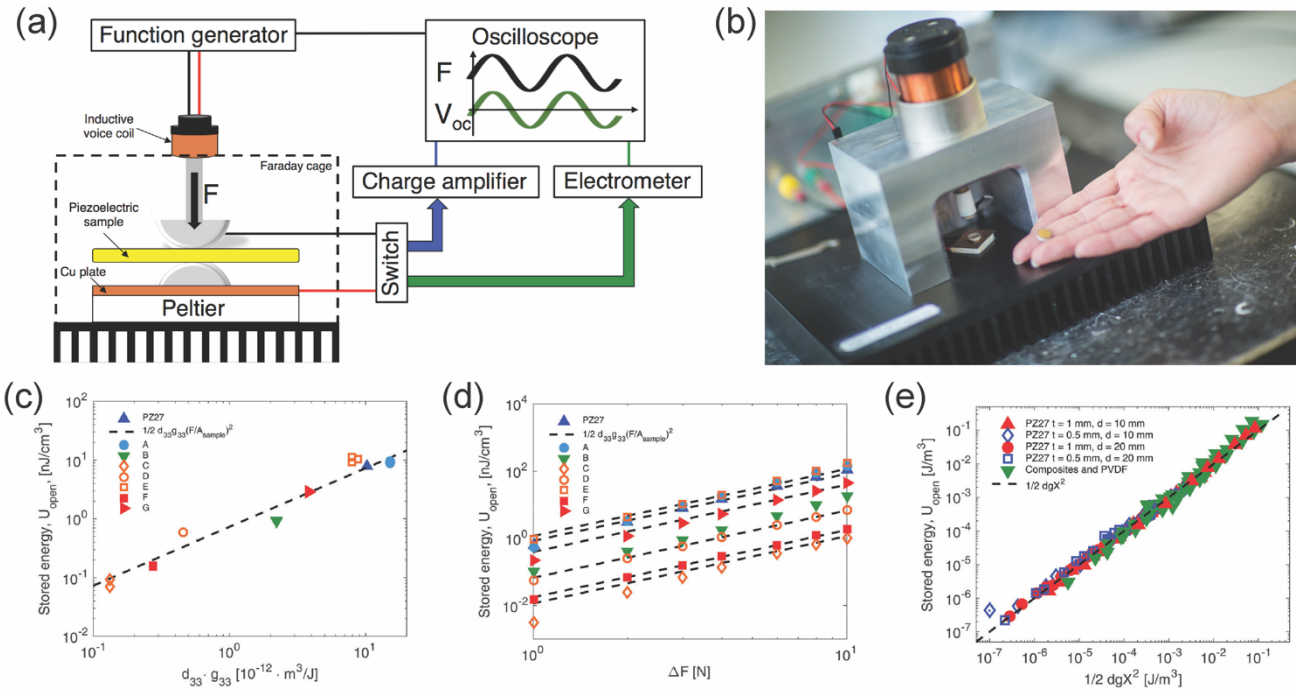

Figure 2: Experimental layout and verification of the piezoelectric FOM. (a) Schematic showing the layout of the purpose-built electrometer for precise mechanical deformation and the subsequent collection of data and (b) a photograph showing the experimental layout. (c) The stored energy plotted as a function of the FOM $g_{33}d_{33}$ for a range of piezoelectric materials including lead zirconate titanate (PZ27, PZT), PZT 1-3 fiber composite in epoxy (A), β phase PVDF (B), randomly distributed 0-3 particle composites from PZT (C, D) and lithium sodium potassium niobate in PDMS (E, KNLN), 1-3 dielectrophoretically aligned particle composites using PZT (F) and KNLN (E). (d) shows the dependence of U_{open} on the input force for the perovskite, fluoropolymer and perovskite-polymer composites and (e) shows the agreement between the model and experimental data for all samples. The modelled data is represented as the black dashed black line in (c-e). Reproduced with permission from ref 51. Copyright 2018, Royal Society of Chemistry.

dependent on the phase.[53] The polymer has been found in five distinct phases, known as α, β, γ, δ and ε.[54, 55] Of those, the α and β phases are the most commonly found. The γ phase is a transitional state between α and β and therefore not as common.[43] The other phases, δ and ε, are more difficult to isolate and not generally found through conventional processing techniques.[55]

The α phase of PVDF has a *trans-gauche* conformation (TGTG´) (Fig. 3a), and hence is non-polar. The β phase consists of all-*trans* conformation (TTTT) (Fig. 3b) meaning the majority of fluorine atoms are separated from hydrogen atoms and hence it possesses a dipole moment perpendicular to the polymer chain (7.0×10^{-30} C m).[56] The third type of chain orientation is the γ phase (Fig. 3c). This orientation is a transitional structure between the α and β phases and hence shows a smaller dipole moment than that of the β phase.[57] This can be explained by its structure, taking on a *trans-gauche* conformation with a higher *trans* fraction (TTTGTTTG´). Thus, of all the chain orientations in PDVF, the β phase shows the highest net dipole moment, suggesting the necessity to increase its proportion within the material to maximize the electrical output of a PVDF-based PEG.

The presence of a dipole moment in the 3 direction of β-PVDF, in combination with the material acting as a dielectric material, allows this fluoropolymer to exhibit electromechanical coupling. As shown in Eqn (8) in the previous section, the contribution of surface charge to electromechanical coupling is dependent on the d_{ip} coefficients, which have been reported in literature for β-PVDF for all three directions of strain. However, discrepancies between the magnitude of values in literature are observed, generally attributed to a varying degree of β phase purity within the polymer, the temperature at which values were obtained and the thickness of the measured film.

Table 1 shows the reported values for d_{ip} in β-PVDF for $i = 3$ and $p = 1, 2, 3$. Here, it is assumed that the polarization vector is parallel to the 3 direction, the electrodes are attached across the 3 direction, i.e., along the surfaces of the films with the highest area, and p accounts for the compressive and longitudinal strains along directions 1, 2 and 3. It has been shown that the d_{33} charge coefficient is the largest due to the compression of the dipole vector directly, whereas d_{31} is smaller as the stretching occurs along the polymer chain orientation axis (indirectly compressing the distance between dipoles). The smallest values are observed for d_{32} because it corresponds to the increase of the distance between polymer chains with low compressibility of the dipole.[45]

The charge coefficient is further dependent on the temperature of the sample, which affects the compressibility of the dipole. Fig. 4a shows the relationship of the coefficient and

Table 1: Selected piezoelectric charge coefficients for PVDF.

Piezoelectric charge coefficient	Experimentally obtained values pC N^{-1}	References
d_{31}	6-20	45, 58
d_{32}	1-4	45, 58
d_{33}	13-28	11, 59-61

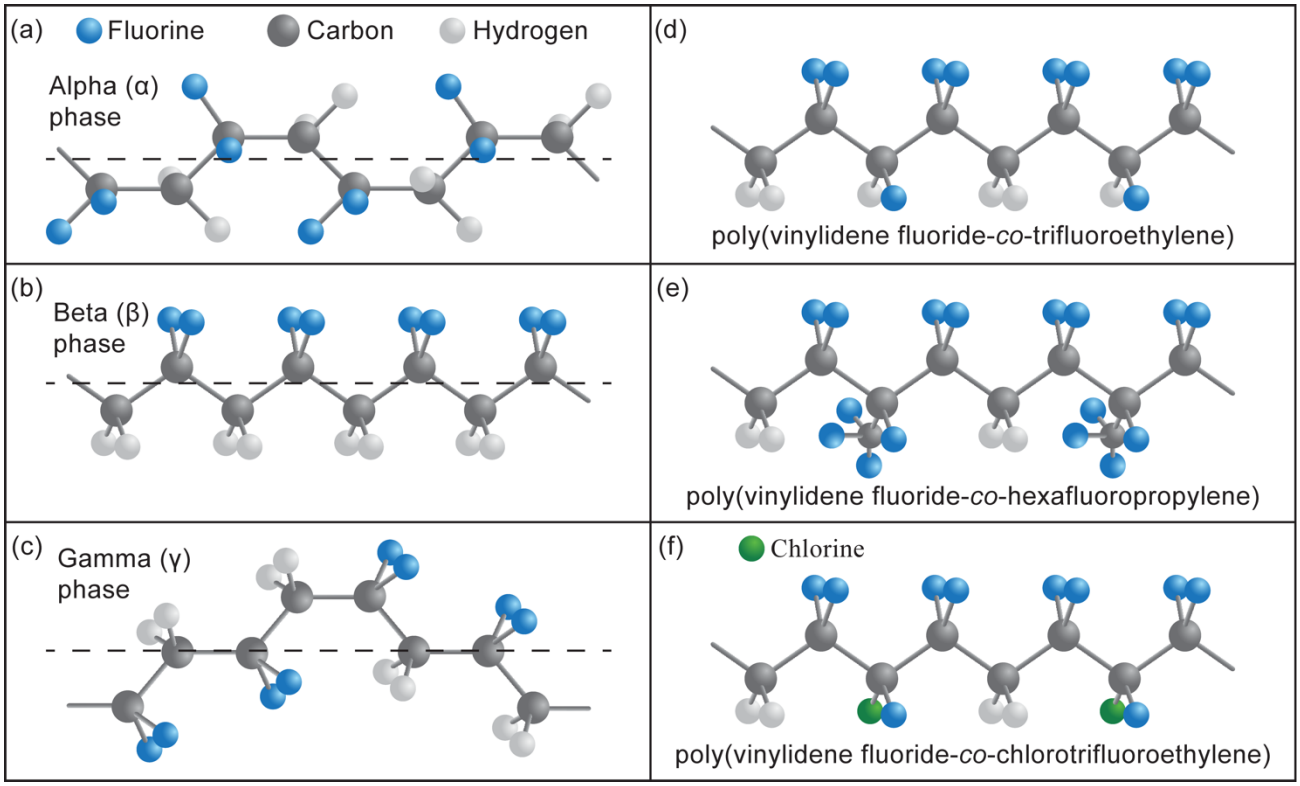

Figure 3: Chemical structure of (a) alpha phase, (b) beta phase and (c) gamma phase conformations of poly(vinylidene fluoride), as well as the chemical structure of (d) poly(vinylidene fluoride-*co*-trifluoroethylene), (e) poly(vinylidene fluoride-*co*-hexafluoropropylene) and (f) poly(vinylidene fluoride-*co*-chlorotrifluoroethylene).

temperature. The study by Destruel *et al*.[58] has found a direct relationship between d_{ip} and temperature, which can be attributed to the chain mobility of the polymer, allowing for a greater net dipole moment change. It is further accepted that the coefficients reduce to zero at the Curie temperature (T_C); therefore, at ambient conditions, PVDF exhibits piezoelectric properties in all deformation directions. This attribute is essential, as the strain cannot be isolated to a single direction in applications related to portable and implantable electronics.

The electromechanical energy coupling coefficients k_{ip} for i = 3 and their temperature dependence are shown in Fig. 4b.[58] Experiments have suggested the coupling factor remains constant between -20 °C and 60 °C when strain is applied in directions 2 and 3. Conversely, an increase in the coupling factor has been observed for the case of strain applied in direction 1 as a function of increasing temperature, deviating from the other directions.

The dielectric constant of PVDF, with a value of ε = 12, is significantly lower than that of conventional piezoelectric materials (i.e., perovskites such as lead zirconate titanate ($Pb[Zr_xTi_{1-x}]O_3$, PZT, ε = 2400) and barium titanate ($BaTiO_3$, BTO, ε = 2479)).[11, 45, 60, 62] Additionally, the spontaneous polarization of pure β-PVDF has been experimentally reported as P_s = 1.32 × 10^{-2} C m^{-2}. The remnant polarization (P_r) of PVDF has further been linked to the thickness of the material, with experiments suggesting an increase in P_r as a function of an increase in thickness. This phenomenon is attributed to a change in the aspect ratio of the material, where the potential difference on a 33-form PEG is given by Eqn (18).

$$V_{Q=0} = \frac{a}{bc} g_{33} F \quad (18)$$

Here, a is the thickness of the material, b and c are the length and width of the material, respectively, and F is the applied force.[63, 64] Hence, as the thickness increases, higher voltage can be observed. The recent review by Uchino[65] has discussed the influence of PEG geometry on the resultant electricity generation, as well as the optimal circuitry on how to measure the electrical output of PEGs.

3.2. Thermal, mechanical and optical properties of PVDF

While the electromechanical coupling is the most interesting property of PVDF, especially within the β phase, other properties are important for its application. For example, requirements of optical transparency, thermal and chemical stability, as well as mechanical flexibility and biocompatibility can play a key role in enabling applications.

PVDF is a thermoplastic polymer, with the electroactive phase melting at approximately 170 °C. The β orientation of PVDF has an increased density (ρ = 1.97 g mL^{-1}) compared to the amorphous PVDF (ρ = 1.78 g mL^{-1}) due to a higher degree of crystallinity and hence higher packing density. The lattice parameters have been determined experimentally for the orthorhombic β-PVDF unit cell, given as a = 8.47 Å, $b = 4.90$ Å, $c = 2.56$ Å.[54] As the glass transition temperature (T_g) of PVDF is between -60 °C and -20 °C, PVDF is a rubbery polymer at all temperatures above 0 °C, irrespective of the phase.[45, 57] Furthermore, all phases of the polymer melt at similar temperatures (T_m), although minor differences in the T_m have

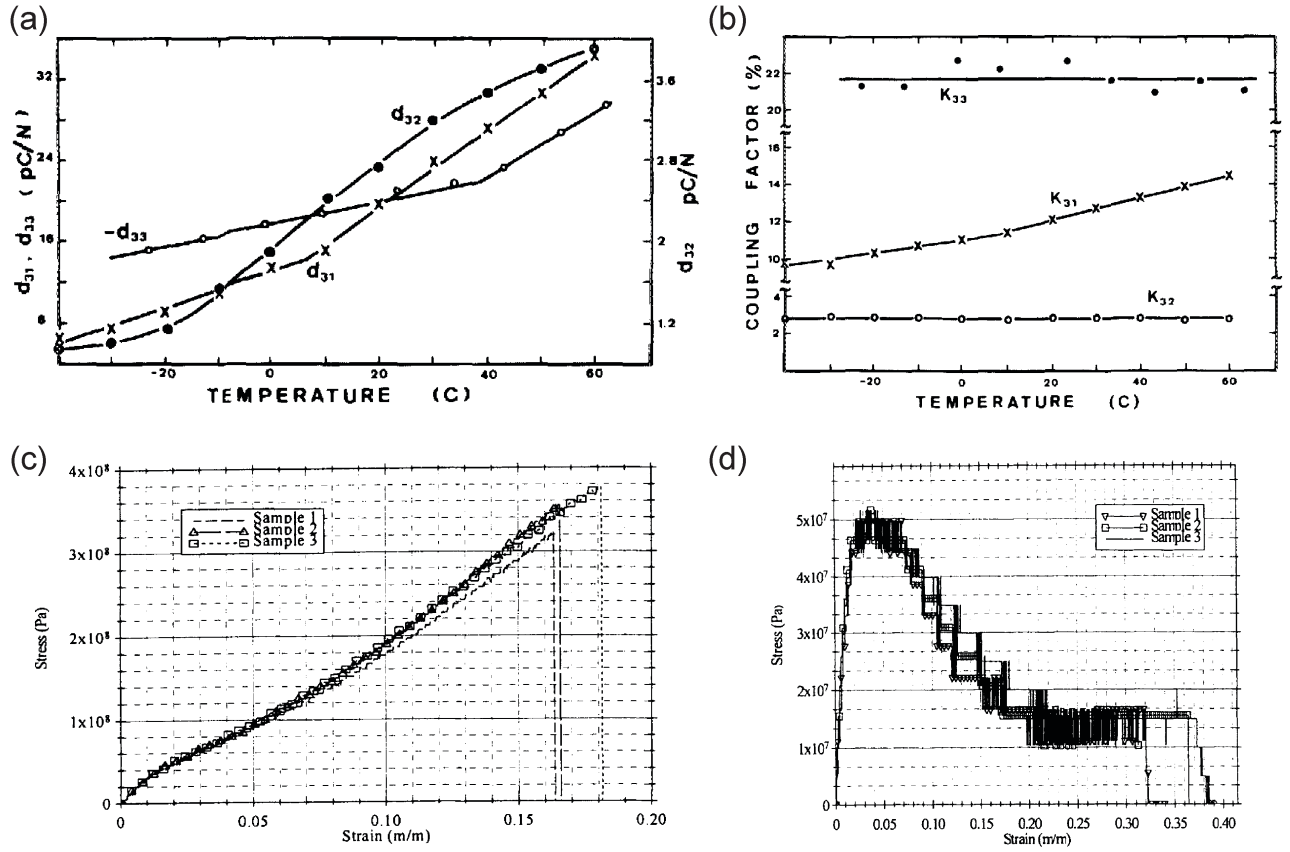

Figure 4: The temperature dependence of the directional (a) piezoelectric charge coefficients d_{ip} and (b) piezoelectric energy coupling coefficients k_{ip}. Reproduced with permission from ref 58. Copyright 1984, American Institute of Physics. Stress-strain response of PVDF in the (c) 1 direction and (d) 2 direction. Reproduced with permission from ref 45. Copyright 1999, Taylor and Francis.

been suggested to be Influenced by the phase. Hence, the value of T_m has been proposed as a characterization tool to discern various crystalline phases and we will discuss this in greater detail in the next section. The T_C of PVDF has been widely debated, however most data suggests it to be above the T_m, between 195 °C and 197 °C.[66, 67] The T_C is regarded as the point when the material loses spontaneous polarization. Therefore, in PVDF this means the polymer chains rotate to reduce the net energy and hence randomize the polarization vector.

In regard to mechanical properties the Young's moduli (Y_i) in various directions *i* of strain for PVDF are similar, where $Y_1 = 2.56 \times 10^9$ Pa for direction 1 (along the axis of the polymer backbone) and $Y_2 = 2.6 \times 10^9$ Pa for direction 2 (perpendicular to the polymer chain orientation and the thickness axis). However, the similarity is only at the initial region of the strain-stress curve, shown in Fig. 4c,d. Past the initial region in the direction 1, the stress-strain curves exhibit behavior typically found in brittle materials (Fig. 4c) — a linear increase in stress as a function of strain up to a maximum, whereby the material fails. Conversely, PVDF shows properties representative of ductile materials in direction 2 (Fig. 4d).[45] Studies on the anisotropic mechanical properties of PVDF suggest that there is a difference of approximately one order of magnitude between maximum stresses ($\sigma_{max,i}$) between directions 1 and 2: $\sigma_{max,1} = 3.5 \times 10^8$ Pa and $\sigma_{max,2} = 5.1 \times 10^7$ Pa.[68, 69]

The optical properties of PVDF are also important. Ideally, the control over transparency, haze and clarity is required depending on the use of the material. The major reason for low visible-wavelength transmittance and high haze in PVDF is surface roughness. Although limited efforts have been made in isolating optical properties and optimal conditions for transparency of β-PVDF, several researchers have studied α- and δ-PVDF.

Li *et al.*[37] has proposed a relationship between the root mean square (RMS) roughness and the optical transparency, clarity and lack of haze in δ-PVDF. The films have been deposited via both Meyer bar coating and spin coating methods at elevated temperatures to decrease surface roughness. Here, post-processing includes applying a short electrical pulse across the attached electrodes to convert the α phase into the δ phase. Further work by the researchers, Li *et al.*,[38] suggest the presence of humidity as the main factor for the presence of haze in films of solvent cast α-PVDF. Further, they report vapor-induced phase transition as the primary cause of high haze and low clarity in solvent evaporation-assisted PVDF deposition methods. Hence, the authors have been able to produce thin films of PVDF with approximately 0% haze, approximately 100% clarity and visible wavelength absorbances below $<10^{-2}$ at 0% relative humidity and 40 °C deposition temperature.

3.3. Comparison of PVDF properties with other piezoelectric materials

It is useful to compare the properties of PVDF to other well-known piezoelectric materials, in order to highlight its suitability

for applications in flexible PEGs. Table 2 shows a selected list of properties for PVDF compared to alternative piezoelectric materials. Materials such as PZT and BTO are perovskite structures, whereby the titanium atom arranges itself in the center of the unit cell and induces spontaneous polarization below the T_C. The d_{33} coefficient in PZT and BTO is one order of magnitude higher than polymer-based piezoelectric materials. These materials are dense in nature (>5 g mL^{-1}) with a high Young's modulus, suggesting their brittleness and limiting their use in applications requiring flexible materials without significant processing.[70-73] The presence of lead in PZT and similar perovskites further limits applications in medical devices due to its toxicity.[39] On the other hand, voided charged polymers (VCPs) such as cellular poly(propylene) (PP) have a comparable d_{33} to perovskite materials. Conversely, VCPs generally have a lower maximum operating temperature, a low conversion from mechanical to electrical energy (k_{33}), low structural integrity and low dielectric constant, limiting their utilization in real-world applications as mechanoelectrical conversion devices.[59]

In contrast to perovskite structures and VCPs, PVDF and related fluoropolymers exhibit a moderate electromechanical conversion efficiency; importantly, they possess an acoustic impedance similar to that of human tissue, making them more suitable for biomedical applications relative to perovskites and VCPs.[74, 75] It is biocompatible as it does not contain toxic lead, unlike many perovskites, in particular PZT.[11] Furthermore, PVDF is flexible with a high Young's modulus relative to that of VCPs, suggesting its improved mechanical strength.[69] Additionally, it can be processed to show high transparency in the visible wavelength region with high clarity and low haze.[37, 38]

Table 2: Physical, dielectric and piezoelectric properties of selected piezoelectric materials, showing perovskites, bulk polymers and voided charged polymers.

Material		PZT[a)]	BTO[b)]	PVDF[c)]	Cellular PP[d)]
References		11, 80	60, 62, 80	11, 59-61	11, 59, 81
Density ρ	g mL^{-1}	7.80	5.72	1.78	0.33
Young's modulus Y	GPa	50-60	116-128	2.5-3.2	0.002
Dielectric constant ε		2400	3279	7.6-12	1.12-1.23
Charge coefficient d_{33}	pC N^{-1}, pm V^{-1}	289-500	105-460	13-28	80-800
Voltage coefficient g_{33}	V m N^{-1}	0.026	0.013	0.320	30
FOM[e)]	10^{-12} m^2 N^{-1}	8-13	1-6	4-9	2400-24000
Coupling factor k_{33}		0.69	0.49	0.20-0.27	0.06
Maximum operating temperature	°C	250	120	90	50

[a)] $Pb[Zr_xTi_{1-x}]O_3$ (PZT), perovskite; [b)] $BaTiO_3$ (BTO), perovskite; [c)] poly(vinylidene fluoride) (PVDF), solid polymer; [d)] cellular poly(propylene) (PP), voided charged polymer; [e)] figure of merit (FOM) from Eqn. (17), given as $d_{33}g_{33}$ (10^{-12} m^2 N^{-1}).

4. Characterization of PVDF

To understand the properties of PVDF, and quantify the phase composition, several characterization techniques have been commonly utilized, including x-ray diffraction (XRD), Fourier transform infrared (FTIR) spectroscopy, differential scanning calorimetry (DSC) and polarity switching measurements are then used to measure the total polarization in the material. More recently Raman spectroscopy has also been employed. This section will highlight these techniques.

XRD, FTIR and DSC are commonly used together to develop an understanding of the contributions of various phases to the microstructure of PVDF. Representative fingerprints of α, β and γ phases can be obtained by these techniques and are shown in Fig. 5(a-c), for XRD, FTIR and DSC, respectively.[56, 68, 76-79]

XRD is commonly used to fingerprint the phases of the polymer.[43] As shown in Fig. 5a, the XRD pattern for β phase shows the combination of a broadened peak at 20.26 ° (2θ) and a weakened shoulder at lower angles. In contrast, the XRD patterns of α and γ phases are noticeably different. The α phase of PVDF displays a sharp peak at 19.90 °, an additional pair of easily resolvable peaks at 17.66 ° and 18.30 °, as well as a feature at 26.56 °. In the XRD pattern of γ phase PVDF, peak broadening occurs and the main characteristic peak shifts to a higher angle of 20.04 °, while the pair of sharp peaks found in α PVDF transforms into a single broad feature located at approximately 18.50 °. The features between 17.66 ° and 18.50 ° in α and γ phases have been attributed to the *gauche* conformation in the structure of PVDF, which is not found in β phase.[82] The XRD method can serve as a qualitative analysis for confirming the presence of pure β phase and distinguishing it from other commonly found phases.

The FTIR characterization is most widely used to determine β phase fraction of PVDF (Fig. 5b). It involves the quantitative comparison of absorbance at 766 cm^{-1} (attributed to α phase) and that at 840 cm^{-1} (attributed to β phase) through Eqn (19).

$$F(\beta) = \frac{A_\beta}{(K_\beta/K_\alpha)A_\alpha + A_\beta} \quad (19)$$

Here, $F(\beta)$ represents the fraction of β phase PVDF, A_α and A_β represent the absorbances at 766 cm^{-1} and 840 cm^{-1}, respectively, and K_α and K_β are the absorption coefficients at the respective wavenumbers with the values given as 6.1×10^4 cm^2 mol^{-1} and 7.7×10^4 cm^2 mol^{-1}, respectively.[83] However, it should be noted that FTIR cannot be used alone to quantify the presence and relative proportions of the phases, due to the peak at 833 cm^{-1} from γ phase PVDF overlapping with the peak at 840 cm^{-1} for β phase PVDF.[84] Many authors suggest that Eqn (19) should be used to determine the total fraction of electroactive phases (β and γ phases combined), as shown in Eqn (20).[85] In this modification, F_{EA} is the total electroactive fraction and I_{EA} is the absorbance at 840 cm^{-1}.

$$F_{EA} = \frac{I_{EA}}{(K_\beta/K_\alpha)I_\alpha + I_{EA}} \quad (20)$$

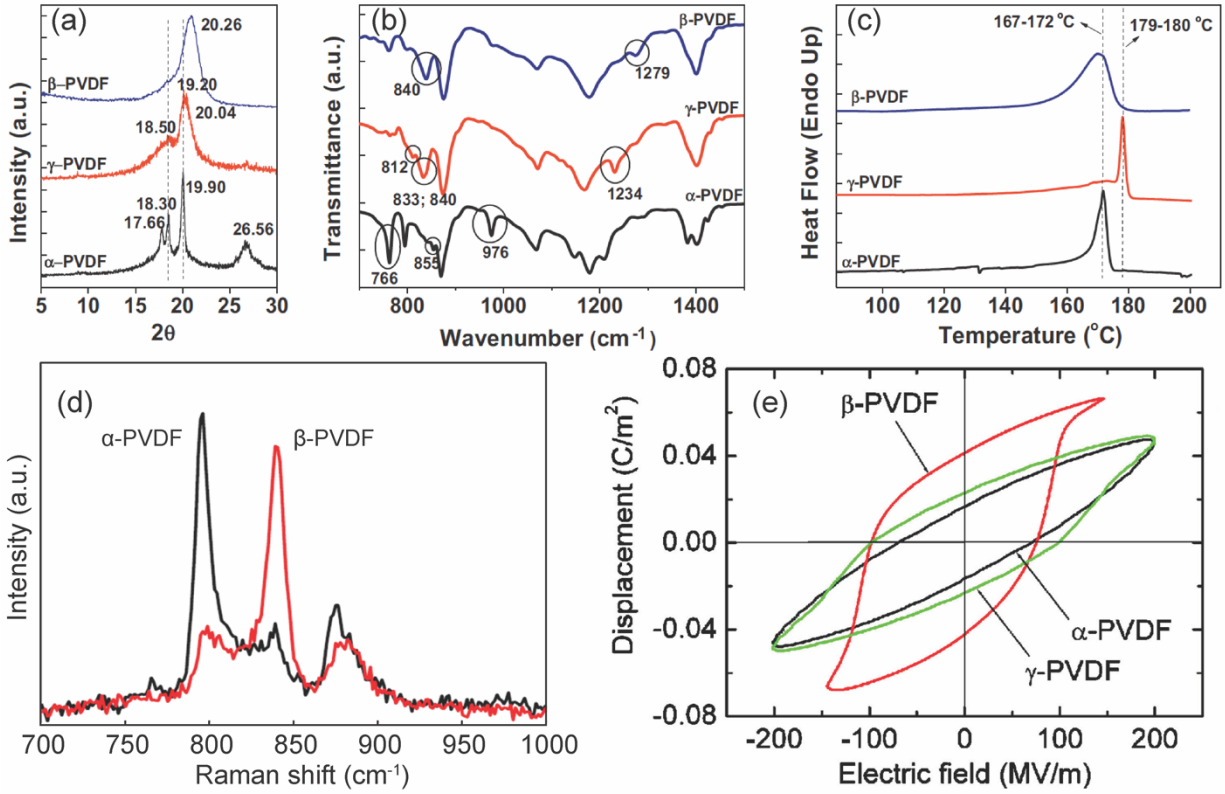

Figure 5: Typical fingerprints of α, β and γ phases of PVDF in common characterization techniques, (a) XRD ($K_{\alpha1}$, λ = 1.5405600 Å); (b) FTIR, (c) DSC, Reproduced with permission from ref 43. Copyright 2014, Elsevier. (d) Raman spectroscopy (λ = 532 nm), Reproduced with permission from ref 78. Copyright 2014, SPIE. (e) electric displacement-electric field (D-E) hysteresis loops, Reproduced with permission from ref 79. Copyright 2010, American Institute of Physics.

Furthermore, to separate the contribution from the distinct electroactive phases, a peak-to-valley height ratio approach has been proposed, whereby the absorbances reflecting the β phase peak at 1275 cm^{-1} and the γ phase peak at 1235 cm^{-1} are used, shown in Eqns (21) and (22).

$$F(\beta) = F_{EA} \times \left(\frac{\Delta I_{\beta'}}{\Delta I_{\beta'} + \Delta I_{\gamma'}}\right) \quad (21)$$

$$F(\gamma) = F_{EA} \times \left(\frac{\Delta I_{\gamma'}}{\Delta I_{\beta'} + \Delta I_{\gamma'}}\right) \quad (22)$$

In this instance, $\Delta I_{\beta'}$ is attributed to the difference in intensity between the β phase peak at 1275 cm^{-1} and the preceding "valley" at approximately 1260 cm^{-1}, and $\Delta I_{\gamma'}$ is attributed to the difference in intensity between the γ phase peak at 1234 cm^{-1} and its preceding "valley" at approximately 1225 cm^{-1}. This method of quantification has been increasingly utilized since its initial reports.[86-88] It should be noted that the peaks for the various phases tend to overlap in FTIR, making quantitative fingerprinting of the phases difficult. Hence, XRD should be used as a secondary characterization method to confirm the presence of β phase and, more importantly, rule out the presence of α and γ phases in PVDF and related fluoropolymers.

In addition, DSC is an alternative method to qualitatively distinguish relatively pure phases from each other, shown in Fig. 5c. Depending on the phase of the material, the endothermic peak related to the relaxation in the polymer chain conformation upon melting shifts to a different position and changes its relative width. Moreover, DSC can be applied as a quantitative technique to measure the enthalpy of melting within the sample, and hence calculate the relative crystallinity using the reference value for the enthalpy of completely crystalline PVDF.[89] In this method, the temperature of melting has been suggested to shift based on the conformation, as shown in Fig. 5c.[43] The enthalpy of melting (ΔH_m) can be calculated from the area under the melting peak on the thermogram and is given as a mass-normalized value with units J g^{-1}. The total crystallinity percentage can then be calculated using Eqn (23).[39]

$$\chi_c = \frac{\Delta H_m}{\Delta H_0} \times 100 \quad (23)$$

Here, χ_c is the crystallinity fraction and ΔH_0 is the literature melting enthalpy the completely crystalline PVDF material with a value of 103.4 J g^{-1}.[68, 89, 90]

In recent times, Raman spectroscopy has been suggested as an alternative method to fingerprint the phases in fluoropolymers. This method was first utilized by Constantino *et al.*[91, 92]. Subsequent work by Riosbaas *et al.*[78] has further popularized this method for discriminative characterization of α and β phases in PVDF. The representative spectra for the samples with predominantly α and β phases are shown in Fig. 5d, and clear differences can be seen between the typical Raman signatures. This publication has attributed the peak at 839 cm^{-1} to the growing amount of β phase upon mechanical stretching of the PVDF films and have suggested the decreasing intensity at 794 cm^{-1} is due to the α phase. Raman spectroscopy

has since been used in an increased number of studies.[93-99] The main fingerprinting region in Raman is found between 700 cm^{-1} and 900 cm^{-1}. The peak at 794 cm^{-1} has been suggested to result from the rocking of CH_2 in the α phase and that at 839 cm^{-1} attributed to the rocking of the β phase CH_2.[91] Furthermore, an additional peak at 812 cm^{-1} has been reported recently due to the influence of γ phase of the polymer.[100] The quantitative analysis of the fraction of β phase relative to that of α phase has been proposed using Eqn (24).[78]

$$\frac{\beta}{\alpha} = \frac{I(\beta)}{I(\alpha)} = \frac{I_{839\ cm^{-1}}}{I_{794\ cm^{-1}}} \quad (24)$$

Here, $I(\beta)$ corresponds to the intensity of the peak at 839 cm^{-1} and $I(\alpha)$ to that of 794 cm^{-1}. A β/α ratio of greater than 1 suggested majority β phase content and below 1 suggested predominantly α phase. Due to the strong and sharp signals in Raman spectroscopy, the peaks do not tend to overlap, hence this technique may be useful in quantifying the relative proportions of the various phases in fluoropolymers.

The presence of a dipole moment in the β phase in the fluoropolymer is a requirement for it to exhibit electromechanical coupling; however, it is not the only requirement. For example, a sample of highly crystalline PVDF with predominantly β phase can exhibit no electrical output if the dipoles are arranged in a random manner, such that the dipole vectors cancel each other (Fig. 6).[101] In this context, a specialized bulk fingerprinting technique for the quantification of a total dipole moment, polarity switching spectroscopy, is used. The measurement generates electrical displacement-electrical field (D-E) or polarization-electrical field (P-E) hysteresis loops as shown in Fig. 5e.[79]

Piezoelectric polymers such as β-PVDF are a special case of dielectric materials, whereby their dipoles remain polarized after an external influence is removed. This gives rise to several critical parameters necessary to quantify the polarizability of fluoropolymers, described in great detail by Damjanovic[44]. The first parameter is spontaneous polarization P_s, which is denoted by the y-intercept of the extrapolation of the final linear region in the hysteresis loop of a piezoelectric material (Fig. 5e), and this parameter quantifies the total possible polarization. Hence, a larger P_s correlates with a higher electrical output of the polymer. The second important parameter, introduced as the y intercept of the hysteresis loop, is called remnant polarization P_r and represents polarization due to oriented dipoles which remain aligned with no external field in the material. For the piezoelectric material to be considered stable, P_r should be comparative to that of P_s. In most real-world scenarios, P_r tends to be lower than P_s due to factors such as temperature and electromagnetic interferences.

The final parameter used in measuring polarization in fluoropolymers is the x-intercept of the hysteresis loop and is generally referred to as coercive field E_C. The physical meaning of this parameter is the electric field required to instantaneously depolarize the material. Measuring these parameters is quite important for optimizing the conditions for post-deposition processing (poling—refer to section 5.4) as well as understanding and enhancing electromechanical properties in PEGs.

The characterization techniques outlined in this section form a basis for understanding the conformational properties of PVDF and its related copolymers. The ability to pinpoint the amount of total crystallinity (Fig. 6a) is important, as it encompasses all non-amorphous phases, which include α, β and γ. Investigation using FTIR, XRD and Raman spectroscopy assists in quantifying the relative proportions of the crystalline phases (Fig. 6b). As outlined previously, the main purpose of the research into PVDF as a piezoelectric polymer able to generate electricity is to increase the fraction of total crystallinity,

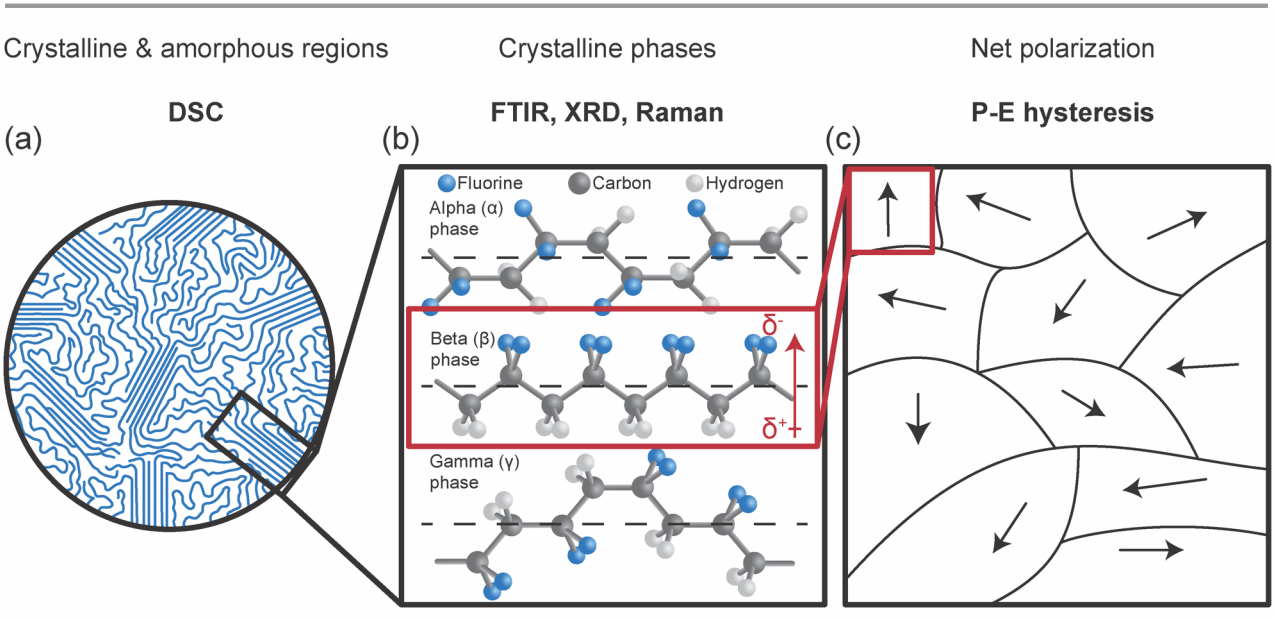

Figure 6: Synopsis of the factors affecting the electrical output of a fluoropolymer PEG and the respective methods used for their characterization.

whereby the β phase within the crystalline portion is maximized. Therefore, these spectroscopic methods are critical for understanding the material. However, to optimize the electrical signal obtained from mechanical deformation of the polymer, the dipole moment direction of all the polymer chains must be oriented in a single direction. Polarity switching measurements are then used to measure the total polarization in the material. Thus, the methods outlined in this section are necessary to understand the various properties of PVDF and related fluoropolymers, in order to tailor the materials for greatest electromechanical conversion appropriate for their uses in PEGs.

5. Control of parameters relating to piezoelectricity in fluoropolymers

For the purposes of translating PVDF-based PEGs into the aforementioned applications, the electrical output of the devices should be maximized. In fluoropolymers, a range of variables can be controlled to either directly or indirectly affect the electrical output of the resultant PEGs. Namely, the choice of polymerization parameters and techniques can increase the purity of the polymer and aid preferential nucleation into the electroactive β phase during later stages of processing. Different polymer deposition techniques also exist and can significantly affect the electrical output of flexible PEGs.

The electrical characteristics of PEGs can be altered by post-deposition processing methods, also commonly known as poling, aimed at increasing polarization within the polymers. Also, the inclusion of various co-monomers can influence the processability and electromechanical coupling effects in resulting copolymers. Lastly, the incorporation of nanomaterials and fillers to make fluoropolymer composites can vary the magnitude of the electrical output due to a range of effects. The following sections discuss each of these in detail.

5.1. Polymerization parameters and techniques

The synthesis route of PVDF plays an important role in the enhancement of the polymer's electroactivity, allowing for increased energy conversion efficiencies. PVDF is a linear chain fluoropolymer consisting of a linear vinyl chain with a difluorine functionality on every second carbon.[102] The polymer is generally synthesized via either a free-radical polymerization or a more controlled method such as reversible addition-fragmentation chain-transfer (RAFT) polymerization from the monomer, vinyl difluoride.[57, 103]

The monomer itself is gaseous at standard atmospheric conditions, hence the polymerization is typically undertaken in an emulsion or in a suspension to maximize yield.[103] The former utilizes water soluble initiators, whereas the latter uses organosoluble initiators coupled with water soluble polymers such as poly(vinyl alcohol) acting as stabilizers for the monomer. It should be noted that the emulsion polymerization is undertaken in a medium with a high heat capacity such as water, which is able to dissipate the heat produced by the polymerization reaction.[104] The documented method of termination of the PVDF polymerization reaction is described as either recombination, through the combination of two active polymer chains, or alternatively hydrogen abstraction from a proton donor solvent if available.[53, 105]

Several works have extensively documented the parameters of PVDF polymerization, including assessments of quality of polymer based on parameter sets.[57, 106] Ameduri[57] and Soulestin *et al*.[107] have written several extensive reviews on the various polymerization techniques and pathways for PVDF and other fluoropolymers, as well as the influence of key parameters during the polymerization on the properties of the resulting polymers. These reviews can be used as a guide for literature surrounding the polymerization parameters.

Due to the nature of radical-initiated polymerization processes, defects have been found in the products, deviating from the desired head-to-tail propagation (Fig. 7a, I).[53] The presence of head-to-head (Fig. 7a, II) and tail-to-tail (Fig. 7a. III) defects has been attributed to polymerization conditions and temperature.[57]

Emulsion-polymerized PVDF has been found to contain a higher proportion of head-to-head defects relative to suspension, with a 3-7 mol% defect proportion in commercially produced PVDF. It has been proposed that decreasing the proportion of defects within the polymer will increase crystallinity, with researchers claiming a low degree of defects (0.73 mol%) in vinylidene fluoride telomers results in a well-organized β phase structure.[108] This data suggests an increased β phase fraction can be obtained with a decrease in the molecular weight of the polymer. However, in PVDF with higher molecular weights, the opposite has been found to occur. In one of the few experiments linking polymerization parameters to the major polymorphic phase in PVDF, Cais *et al*.[109] have studied the effects of induced defects in the polymer during synthesis and correlated their values to the major phase (Fig. 7b). The authors report the α phase to be the most stable at 11% head-to-head additions and below. However, the β phase of PVDF becomes more stable than the α phase at 15% defects and remains the dominant phase for all analyzed data up to 23% defects.[109] It has been further noted that the melting temperature of PVDF decreases from 180 °C at 3.5% defects (inherent to polymerization of VDF) to 122 °C at 15% defects, with further increases up to 140 °C at 23% defects.[110]

As discussed in Section 3.3, the preferential β phase formation of PVDF is one of the parameters to be maximized for the increased electrical output of fluoropolymers. Hence, the high head-to-head defect fraction at 23% is linked to enhancements of the electrical output of PVDF-based flexible PEGs. In the current state, it is difficult to examine polymerization parameters and their effects on the electromechanical coupling of the fluoropolymers due to a lack of relevant literature. The research in this area is expected to evolve in the near future and will be one of the key areas in enabling commercialization of fluoropolymer-based flexible PEGs.

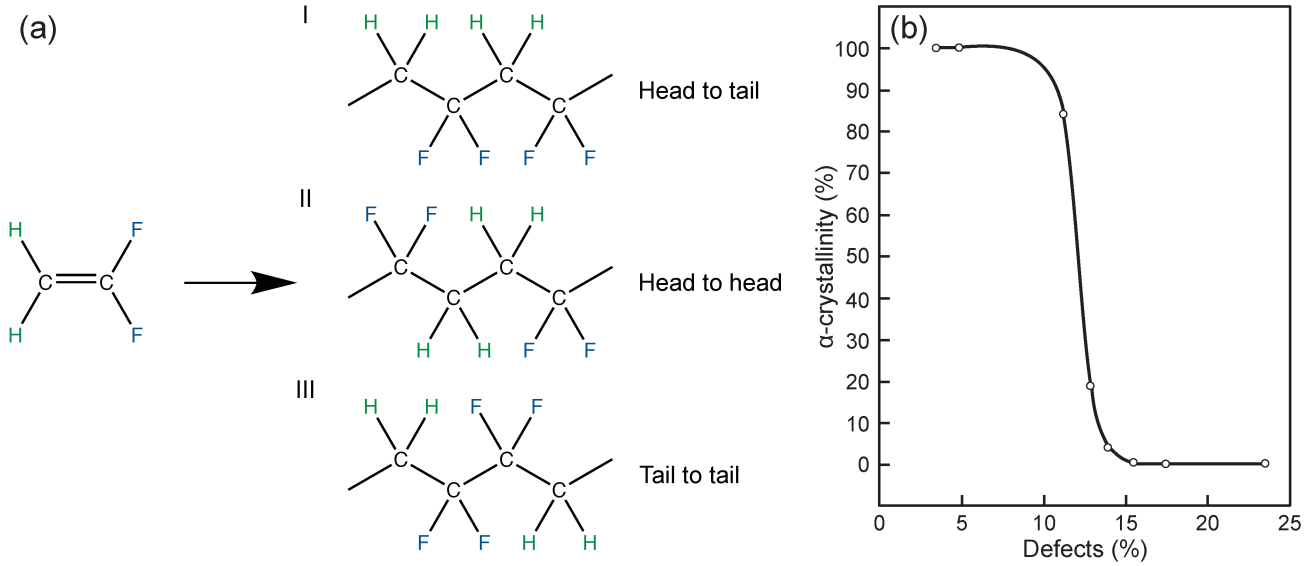

Figure 7: (a) Isomers of PVDF through polymerization of vinylidene difluoride. Head-to-tail propagation (I) is the desired result, however head-to-head (II) and tail-to-tail (III) additions can occur as defects. (b) The fraction of α-phase polymorphs relative to the β-phase in PVDF synthesized with increasing head-to-head and tail-to-tail defect concentration. Reproduced with permission from ref 110. Copyright 1987, Elsevier.

5.2. Co-monomer influences in fluorinated polymers

One of the main downsides of PVDF is low electromechanical coupling relative to perovskites, manifested in its moderate piezoelectric charge coefficient d_{33}, as well as difficulty to process it into the β phase.[43, 111] To counteract these shortcomings, various polymer blends have been developed utilizing alternative fluorinated co-monomers.[57] The commonly studied copolymers of PVDF are presented in this section, and Table 3 lists their electromechanical and dielectric properties for optimized molar fractions of comonomers.

It is clear that variation of these polymers leads to variation in the electrical output of the PEGs based on these blends (Table 3). Maximization of d_{33} and g_{33} is required for increased conversion efficiencies in these copolymers.

A wide variety of copolymers have been synthesized by incorporating vinylidene difluoride with trifluoroethylene (TrFE), hexafluoropropylene (HFP) and chlorotrifluoroethylene (CTFE) co-monomers.[43] The choice of co-monomer, as well as relative ratios of each, leads to tailoring of properties such as T_m, T_g, Young's modulus, dielectric constant, stability and crystallinity, amongst others.[57] Copolymers, with optimized co-monomer ratios, have been shown to deposit as an electroactive phase due to steric effects and dipole-dipole interactions. The reason for changes in the polymer properties is the modification of the symmetry of the polymer and varying the intramolecular and intermolecular forces.

A review by Soulestin *et al*.[107] reports on the effects of the copolymer chemistry on the properties of fluoropolymer copolymers and readers are directed towards their publication for an in-depth discussion on the topic.

The most studied copolymer is poly(vinylidene fluoride-*co*-trifluoroethylene) (PVDF-TrFE) (structure shown in Fig. 3d). In this system, the relative molar ratio of VDF has been experimentally varied in free radical polymerizations.[117] Previous works have suggested successful conversion at all ratios, however only ones containing between 93 mol% and 50 mol% VDF have been produced on a commercial scale.[57]

The addition of the third fluoride atom into the vinyl backbone has been shown to enhance crystallinity in the resultant polymer due to its large steric hindrance relative to the hydrogen it replaces.[118] The favored conformation is all-*trans* and therefore the β phase is the most prevalent in PVDF-TrFE when the VDF is in the range of 50 mol% and 80 mol%.[119, 120] In this range, the T_m of the PVDF-TrFE is lower than that of PVDF, with a T_c between 55 °C and 128 °C (compared to PVDF at 196 °C).[121] The introduction of the TrFE monomer in molar ratios between 25 mol% and 30 mol% has been shown to selectively obtain thin films with high β phase fractions.[107] In terms of the electroactive properties of PVDF-TrFE, the remnant polarization has been determined to be P_r = 110 mC m^{-2}, much higher than that of PVDF (P_r = 80 mC m^{-2}), leading to a higher k_{33}.[9, 112]

Table 3: Comparison of the piezoelectric metrics and coefficients of various PVDF-based copolymers

Electroactivity coefficient	PVDF	PVDF-TrFE 30 mol% TrFE	PVDF-HFP 10 mol% HFP	PVDF-CTFE 12 mol% CTFE
Refs	10, 11, 60, 112, 113	80, 112	114, 115	113, 116
P_r (mC m^{-2})	80	80-110	26-30	28
P_s (mC m^{-2})	120	120-130	26	80
E_C (MV m^{-1})	80-100	50-70	52	100
g_{33} (V m N^{-1})	0.32	0.38	-	0.40
d_{33} (pC N^{-1})	13-28	38	5.4-32	140
k_{33}	0.20-0.27	0.29	0.14-0.36	0.39
FOM[a)]	4.2-9.0	14.4	-	56.0

[a)] figure of merit (FOM) from Eqn. (17), given as $d_{33}g_{33}$ (10^{-12} m^2 N^{-1}).

The copolymer incorporating the hexafluoropropylene functional group as a co-monomer, poly(vinylidene fluoride-co-hexafluoropropylene) (PVDF-HFP), has also been reported to exhibit electromechanical coupling properties (shown in Fig. 3e).[114, 122-124] The HFP group is significantly larger than the TrFE group, hence lower HFP molar ratios are required for the manufacture of semi-crystalline copolymers, induced by steric hindrance.

PVDF-HFP shows semi-crystalline properties at HFP ratios below 20 mol% relative to the VDF monomer.[125, 126] The optimal ratio for the utilization as flexible PEGs has been shown to be between 5 mol% and 15 mol% HFP.[127] Interestingly, PVDF-HFP has been reported to exhibit a larger longitudinal piezoelectric charge coefficient (d_{31} = 43.1 pC N^{-1}) than its thickness piezoelectric charge coefficient ($|d_{31} / d_{33}| > 1$).

Of all the copolymers highlighted in this review, PVDF-HFP has the lowest remnant polarization ($P_r \approx 30$ mC m^{-2}), however the d_{33} coefficient has been reported as up to -32 pC N^{-1}, higher than that of pure PVDF.[115] To the best of the author's knowledge, no value for the g_{33} coefficient has been presented in prior literature, hence the FOM for the 33 direction cannot be calculated. The 31 directionality of PVDF-HFP with 10 mol% HFP has been analyzed for its electromechanical coupling properties by Sukwisute *et al*.[128], suggesting a FOM of 8.8 pm^2 N^{-1} with a d_{31} of 28.7 pC N^{-1}. These values are similar to those of pure PVDF in the 33 directionality, although significantly lower for the use of this copolymer in flexible PEGs.

Another copolymer with reports of enhanced piezoelectric activity is poly(vinylidene fluoride-*co*-chlorotrifluoroethylene) (PVDF-CTFE), the structure for which is shown in Fig. 3f. In this structure the co-monomer replaces a hydrogen atom along the vinyl backbone with a chlorine atom, which provides steric hindrance at specific monomer ratios in the polymer, between 70 mol% and 93.4 mol% VDF.[129] Between these molar ratios, the copolymer is predominantly crystalline. PVDF-CTFE exhibits a T_g between that of PVDF (approximately -40 °C) and PCTFE (approximately 45 °C), based on monomer ratios[57] and is a thermoplastic at VDF fractions above 70 mol%.[130]

One previous study has reported the highest electromechanical efficiency of PVDF-CTFE between 91 mol% and 88 mol% VDF, with the piezoelectric charge coefficient as high as d_{33} = -140 pC N^{-1}. This is significantly higher than any previously reported fluoropolymer.[116] Based on the report of the extraordinarily high d_{33} in this polymer, the electromechanical properties of PVDF-CTFE make it potentially very attractive as an alternative to low-output piezoelectric polymers such as PVDF. However, to date there is limited literature on this polymer; therefore, there is scope for broader studies on this system going forward. Of particular interest are studies on the piezoelectric properties of PVDF-CTFE, as well as studies on PEGs fabricated from this copolymeric system.

5.3. Fluoropolymer deposition and processing techniques

The properties of PEGs are highly dependent on the processing technique of their fluoropolymer components. An overview of the processing techniques and the various applications of PVDF has been recently published elsewhere.[43, 54] Here, we provide a more specialized discussion of deposition and processing techniques in the context of flexible PEGs. Conventionally, PVDF is deposited in a non-polarized manner due to thermodynamic minimization of energy. This randomly oriented polymer needs to be processed post-deposition through the process called poling, whereby the randomly oriented dipoles of the β phase are rotated and aligned in a single direction through the application of an external electric field. The poling process will be discussed further in the review. Firstly, let us consider suitable deposition techniques for fluorinated polymers.

The most common starting conditions for processing and deposition of PVDF into a predominantly β phase material are (1) the melt, (2) solution, (3) α phase solid and (4) composite systems (discussed separately in Section 5.5).[43] Melt extrusion of PVDF is a well-defined process and the most viable in commercial settings. This is evidenced by current commercial availability of materials from Measurement Specialities Inc., Kureha and Arkema Inc. in the form of thin films with thickness between 9 μm and 250 μm.[41]

PVDF films produced from the melt tend to exhibit low β phase fraction.[131] The β phase can be maximized through either a quenching and annealing treatment, stretching and annealing, poling of the α phase films, or a combination of the above.[132, 133] Uniaxial drawing as a processing technique has been reported to yield high fractions of β phase, however further studies have suggested the need for poling as the drawn films are not polarized.[134] The β phase is prevalent in the produced films, although it is not oriented and hence the polarization vector parallel to the thickness axis has low magnitude.

The method of extrusion coupled with immediate uniaxial drawing has been commercialized by Measurement Specialities[41], whereby the films show a piezoelectric charge constant d_{33} = -33 pC N^{-1}, an attractive value for pure PVDF, after the polarization process. However, the coupling factor for the films is low relative to literature values, k_{33} = 0.14 (with respect to typical values between 0.20 and 0.27 in PVDF).[41]

High pressure, high temperature quenching has been previously suggested as a viable alternative to uniaxial drawing, undertaking the treatment at 500 MPa and 280 °C, respectively.[135] This method has resulted in the deposition of a mixture of α and β phases; however, more recent studies at higher pressures show the formation of pure β phase[136], and a mixture of β and γ phases[131]. A study of the dependence of increasing pressure on the fraction of β phase suggests that an enhancement in the β phase fraction occurs with increasing pressure, from 0% at 200 MPa to 85% at 700 MPa.[137] Furthermore, these authors have established temperature-pressure dependence curves for the melting and crystallization of the various phases of PVDF, as shown in Fig. 8. However, for the produced films to show piezoelectricity, and thus be used in PEGs, they are still required to be poled by the application of high voltages, in the range between 100 MV m^{-1} and 400 MV m^{-1}, which is an undesirable post-processing step.[138]

A variety of methods of processing PVDF into the β phase from solution have been proposed, including solvent casting,

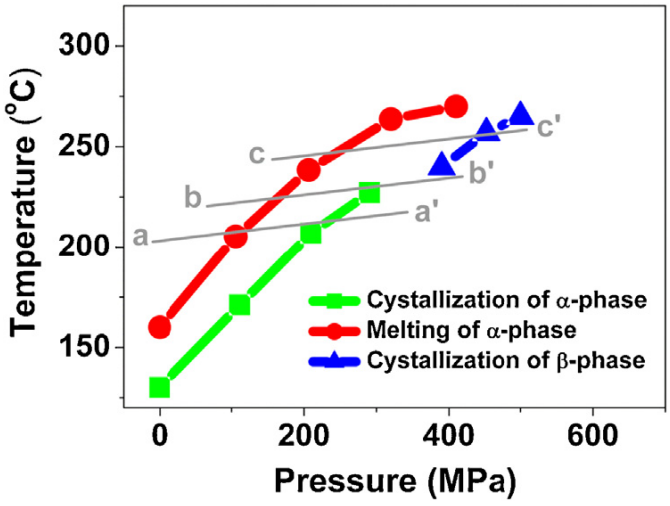

spin coating, electrospinning and Langmuir-Blodgett technique.[43, 54] Recent progress in 3D printing techniques has also allowed for 3D microprinting; however, this technique has led to limited reports to date.[32]

Solvent casting and spin coating have been found to produce films consisting primarily of α phase at near-ambient temperatures, which then require post-processing to convert to β phase.[11, 139, 140] Alternatively, electrospinning and Langmuir-Blodgett techniques yield β phase directly under optimized conditions. These techniques use solvents that can readily dissolve fluoropolymers, such as *N,N*-dimethyl formamide (DMF), *N,N*-dimethylacetamide (DMAc) or dimethyl sulfoxide (DMSO).[38] The boiling points for these solvents are high (>150 °C) and are therefore unsuitable for processing large quantities of polymer solutions at low temperatures.[141, 142] Due to this, swelling agents of PVDF with high volatility such as acetone have been utilized as co-solvents to decrease the drying time of the polymer and improve scalability of the final devices.[32] Solvent systems with boiling points below 100 °C and relatively low toxicity have been reported to dissolve fluoropolymers, which hold potential in utilization where polymer solutions are required for processing.[143]

Solvent casting is the conventional method for the deposition of freestanding polymer films and has been widely utilized and characterized in the field of water-filtration membranes.[144] It is a low energy technique and has potential for commercial roll-to-roll production. The films prepared from this technique show high fractions of α phase and exhibit low piezoelectric properties. They are required to be converted into the β phase through uniaxial drawing (described previously) and reoriented for increased polarization through electrical poling.[11]

Similarly, spin coating allows for materials to be deposited without heating; however, the deposition occurs in the α phase requiring further processing. Spin coating also shows low potential for scalability.

The formation of β phase has been reported on silicon wafers through spin coating, whereby the spin speed and relative humidity were claimed to affect the β phase formation.[142] Secondary effects from the substrate crystallinity could have aided to the crystalline nature of the films.

Electrospinning has been proposed as an alternative technique, whereby a PVDF solution is extruded through a fine nozzle onto a substrate.[102] During the process, a high potential difference of approximately 15 kV is applied between the nozzle and the substrate.[145] The resulting material consists of nano- to micro-scale fibers of PVDF deposited randomly to form low density mats.[74] This technique combines the deposition and poling processes into a single step, with β phase fractions of up to 86%.[146] A rotating collector is commonly used in order to increase the β phase content. The rotation of the collector acts in a similar manner to uniaxial drawing, and the effect depends on the speed of rotation. For example, Ribeiro *et al*.[147] have shown that an increase of the drum speed from 500 rpm to 740 rpm results in a β fraction content between 45% and 85%. Increased spin speeds of the collectors have shown little change in the β fraction.

Electrospinning is limited by the flow rates of the solution, which are commonly between 1 μL min^{-1} and 100 μL min^{-1}.[145] In our opinion, this represents a potential weakness for scalability in fabricating β phase of PVDF; however, other recent reviews have expressed alternative views, describing pilot-scale equipment with possible commercial uses.[148]

Mokhtari *et al*.[149] have reviewed in-depth the literature on the topics of electrospinning and electrospraying of PVDF PEGs, providing an overview of literature up until 2014. Since then, further progress has been made in the optimization of parameters and maximizing electrical generation based on electrospinning fluoropolymers and this review will focus on that literature.

Shao *et al*.[150] have reported on the electrospinning of a nanofibrous PVDF mat with a high β phase content, able to generate a voltage of 2.2 V and current of 2.3 μA under a load of 10 N (Fig. 9a,b). However, the authors have not stated whether the values were collected at a load resistance or at open circuit voltage and short circuit current conditions.

Bin *et al*.[151] have shown that high drum collector rotating speeds can improve the V_{OC} of electrospun PVDF due to highly aligned nanofibers (Fig. 9c). The study reports an increase in V_{OC} from 2 V in mats collected on a stationary drum to 9 V (Fig. 9d) in mats collected at 2400 rpm (754 m min^{-1}), whereby the β phase fraction and the crystallinity have not been found to change.

Hu *et al*.[152] have reported a linear correlation between the "content of effective piezo-phase" (the product of the beta phase fraction from Eqn (19) and the crystallinity from Eqn (23), the $F(\beta) \times \chi_C$) and the electrical output of electrospun PVDF mats (Fig. 9e,f). This study shows that the optimal conditions for the maximization of the content of effective piezo-phase are for a 15 kV needle-to-collector voltage and a collector rotation of 500 rpm (157 m min^{-1}), shown in Fig. 9e. Here, the β phase fraction and the crystallinity are shown to be 87.8% and 71.3%, respectively. The corresponding maximum voltage is reported

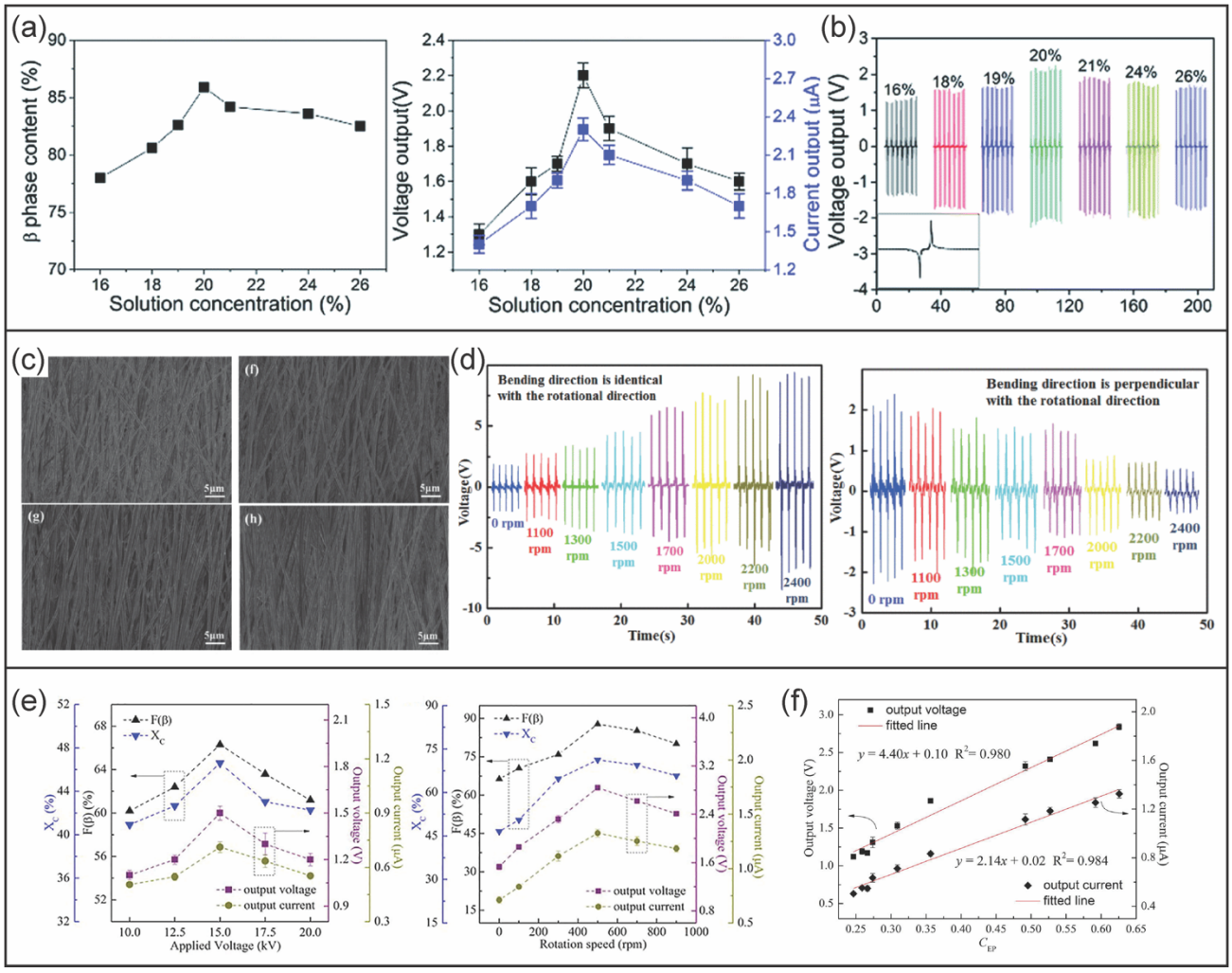

Figure 8: Properties of electrospun fluoropolymer-based PEGs: (a) the β-phase fraction and the corresponding voltage and current outputs as a function of the concentration of PVDF in a solution of *N,N*-dimethylformamide and acetone (40:60 vol%) upon cyclic compression with 10 N force and 1 Hz frequency. Reproduced with permission from ref. 150. Copyright 2015, Royal Society of Chemistry. (c) The alignment of electrospun PVDF nanofibers with increasing rotational speed and (d) the electrical output of the resultant PEGs. Reproduced with permission from ref. 151. Copyright 2015, IEEE. (e) The crystallinity, β phase fraction, output voltage and current as a function of the applied voltage during electrospinning (left) and the rotational speed (right), as well as the electrical generation characteristics for electrospun mats as a function of the content of electroactive phase. Reproduced with permission from ref. 152. Copyright 2018, Elsevier.

as 2.8 V with a current of 1.32 μA (Fig. 9f), compared to approximately 1.6 V and 0.75 μA obtained from a PEG deposited onto a stationary collector.[154] With a piezoelectric layer dimensions of 3 cm^2 area and 50 μm thickness, the maximum volumetric power density in this study corresponds to 154 μW cm^{-3}. Clearly, there is scope to utilize this technique for the production of highly effective flexible PEGs with low volume. Further improvements in the scalability of this method could potentially see it being utilized on a commercial scale.

Thin films have also been made using the Langmuir-Blodgett (LB) technique.[153, 154] In this method, a monolayer of PVDF is floated on the surface of ultrapure water with the help of an amphiphilic stabilizer such as poly(*N*-dodecylacrylamide), forming hydrogen bonds between the fluorine groups in PVDF and the hydrogens in water (Fig. 10a).[155] The monolayer is then adsorbed onto the surface of a substrate by immersing the substrate in water. This technique can be repeated until a desired thickness is obtained, it also removes the need for poling.[156]

The LB method has found to produce nanoscale films of pure and oriented β phase PVDF and PVDF-TrFE.[154, 155] These films have been well-characterized in terms of their compositional[157], optical[154], morphological[154, 158, 159] and piezoelectric[154, 159] properties. PVDF-TrFE thin films produced by the LB technique show a quasi-monolayer formation behavior, approximately 3.5 nm in thickness and a RMS roughness of 3.1 nm for one layer.[154] The thickness of a PVDF LB single-layer film is approximately 2.3 nm.[155] The thickness of a PVDF-TrFE layer is therefore 35% higher than that of PVDF, which has been justified by the steric hindrance of the additional fluoride atom in the TrFE co-monomer and hence the larger unit cell structure.[154]

The remnant polarization of PVDF 30-layer LB film (35 nm thickness) is 60 mC m^{-2}, whereas that of 5-layer (18 nm thickness) PVDF-TrFE is slightly lower at 50mC m^{-2}. It should be noted that the values for E_C increase drastically with a decreasing thickness, between 500 MV m^{-1} and 2.5 GV m^{-1} in single layer PVDF films.[160] The voltage required to switch the polarity of the fluoropolymers are nonetheless low, as the

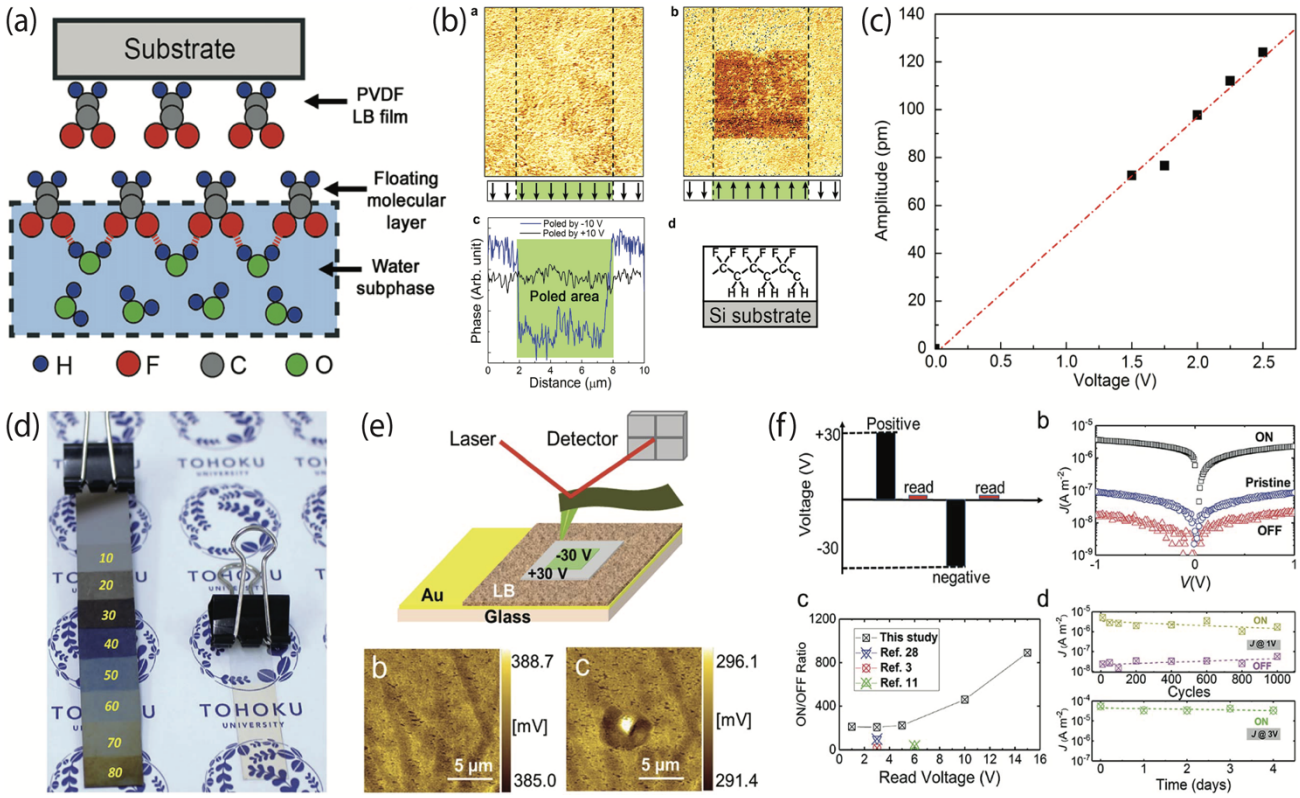

Figure 10: (a) Schematic of orientation of PVDF molecules on water surface and subsequent adsorption onto the substrate surface for the formation of a Langmuir-Blodgett film, (b) piezoresponse force microscopy (PFM) images after applying a positive (left) and negative (right) voltage across the cantilever and the subsequent phase as a function of distance (bottom left), and (c) the change in amplitude measured as a function of applied voltage using PFM, whereby the slope of the line represents the thickness-axis piezoelectric charge coefficient d_{33}. Reproduced with permission from ref 155. Copyright 2012, Elsevier. (d) image showing the colour of the PVDF/P3CPenT (23 wt%) stacked LB monolayers as a function of layer amount on a silicon substrate (left) and a 30-layer LB film on a PET substrate (right), (e) schematic outlining the switching process (top), and the resultant Kelvin probe force microscopy (KPM) images before (left) and after patterning (right), and (f) switching and reading properties for the non-volatile memory devices utilizing PVDF. Reproduced with permission from ref 161. Copyright 2018, Royal Society of Chemistry.

thickness is on the order of nanometers. This is evidenced by piezoresponse force microscopy (PFM) images of an LB surface with an area patterned by applying a voltage to the cantilever, shown in Fig. 10b. The piezoelectric charge coefficient for 20-layer (29 nm thickness) PVDF LB films is d_{33} = -49.4 pC N^{-1} (Fig. 10c), higher than reported elsewhere in literature.[140] Despite the high charge coefficient, these properties are achieved in ultra-thin films (< 30 nm) after the deposition of 20 layers, implying limitations in scalable production of the LB technique, hence it can be used only in special nanotechnology applications.

For example, Zhu *et al*.[161] have utilized PVDF in a blend with a semiconductive polymer, P3CPenT, for a nanoscale non-volatile memory device deposited via the LB technique (Fig. 10d-f). The polarity switching properties of PVDF are utilized for the writing aspect, undertaken via applying a potential difference +30 V for the "ON" state and -30 V for the "OFF" state (Fig. 10e). The two states have been patterned into the 40-layer (104 nm thickness) LB films and the authors report an ON/OFF ratio of approximately 200 when read at 1V, increasing to 891 at 15 V (Fig. 10f), suggesting a high potential for the use of such polymer blends in flexible nanoscale electronics. Obtaining films with micron scale thicknesses, required for generating electricity in practical PEGs, becomes a tedious process and difficult for scale-up to commercial quantities using this technique.

Recent progress in 3D printing technologies has allowed for smaller extrusion nozzles, able to deposit polymers with high precision and resolution.[162, 163] 3D printing utilizes two main modes of operation: melt-extrusion mode, whereby a polymer filament is heated past its melting temperature and pushed through a fine nozzle, and solvent-evaporation mode, where a piston extrudes a concentrated polymer solution through a fine nozzle and the solvent subsequently evaporates.

Melt-extrusion has now been utilized for a multitude of polymeric materials and there is obviously scope and opportunity for printing PVDF structures using this technique.[164, 165] At the time of writing, several companies have released PVDF-based filaments using melt-extrusion 3D printing; however, these tend to be used where chemical resistance is needed, as opposed to for PEG applications. The filaments produced are rigid and opaque in nature.

To date, solvent evaporation-assisted 3D printing for the production of piezoelectric materials for PEGs, has only been undertaken by one research group.[31] Here, they utilize a nanocomposite matrix of BTO in PVDF.[32] In this technique, the solution is extruded using pressure, inducing high shear at the walls of the nozzle. Increased shear forces have previously been shown to produce β phase PVDF.[166] Hence, this process shows

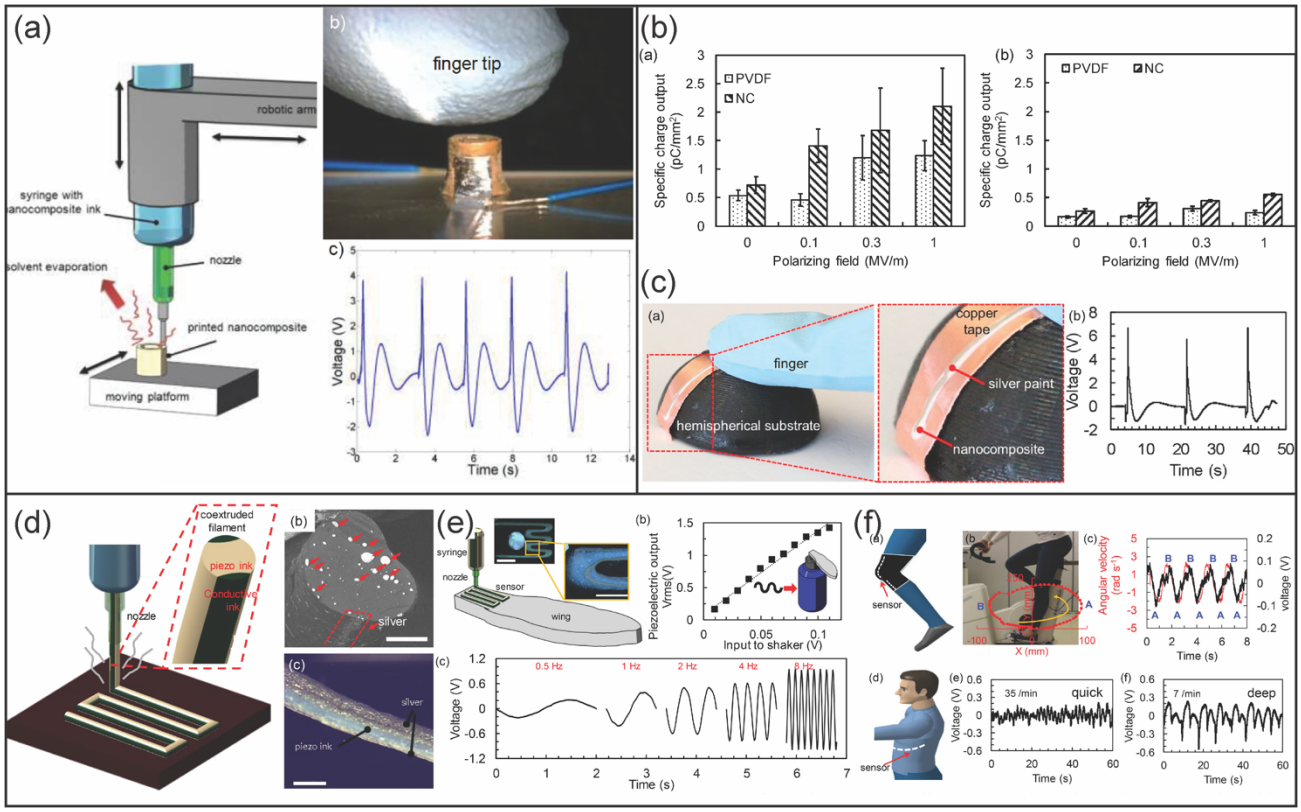

Figure 11: Recent progress in solvent-evaporation assisted 3D printing of fluoropolymer-based PEGS: (a) left, schematic outlining the printing process, right, optical image of the 70-layer composite 31-mode PEG consisting of 10 wt% BTO in PVDF and its respective voltage output upon tapping with a finger, (b) the specific charge output for printed 10 wt% BTO/PVDF composite film with increasing applied potential difference between the nozzle and the substrate, with the right hand panel showing the specific charge output of a single printed film after one year, (c) optical images showing a conformally-printed BTO/PVDF PEG on a copper substrate with a deposited silver paint top electrode and its electrical output upon finger tapping. Reproduced with permission from refs 32 and 168. Copyright 2017 and 2018, American Chemical Society. (d) Schematic showing the 3D printing technique for coextrusion of the silver-coated BTO/PVDF composite ink, with SEM micrographs showing the cross-section of the filament (red arrows indicate BTO agglomerates and dashed border indicates the silver electrode), (e) schematic showing the printing process for a wing-like composite PEG, along with the peak-to-peak voltage output as a function of input to an electromagnetic shaker (right) and the voltage signal over time as a function of frequency (bottom), and (f) a proof-of-concept PEG to harvest energy from the knee during exercise (top left) with the corresponding output voltage (top right) and energy harvesting from breathing, showing the generated voltage as a function of time for quick (bottom left) and deep (bottom right) breathing. Reproduced with permission from ref 169. Copyright 2018, Wiley.

potential in regards to fabrication of piezoelectric structures and is scalable as a part of the fast-growing additive manufacturing industry.[74, 167]

The initial work utilizing solvent evaporation-assisted 3D printing, undertaken by Bodkhe *et al*.[32], has printed up to 70 layers of the material from a mixture of DMF and acetone (Fig. 11a). The nozzle has an internal diameter of 100 µm, which is used to deposit a cylindrical structure with a piezoelectric charge coefficient d_{31} = 18 pC N^{-1} without the use of poling (described in the next section). This group has additionally reported the re-orientation of the polymer chains in the material during printing by applying a potential difference up to 1 MV m^{-1} between the nozzle and the substrate (Fig. 11b).[168] In the printing of single-layer structures, increasing the electric field did not show significant changes in the β phase fraction; however, the specific charge output has been reported to increase both in the PVDF and in the PVDF-BTO samples with the highest at 1 MV m^{-1} for both materials. The study has further demonstrated the 3D printing of patterns and more advanced structures, such as circular and square spirals up to 40 layers and mesh scaffolds up to 9 layers, although their electromechanical properties were not presented. Additionally, a conformal composite printed PEG has been placed onto a hemispherical substrate and upon pressing with a finger has generated a peak voltage of approximately 6.5 V (Fig. 11c).

The latest study by Bodkhe *et al*.[169] has introduced the single-step printing of a one-dimensional PEG via co-extrusion of the previously reported PVDF-BTO composites with a commercially available silver ink on two opposite sides of the piezoelectric material (Fig. 11d). This type of PEG has been reported to generate a voltage of up to approximately 1.5 V when it is attached to a polymer substrate and strain is induced by an electromagnetic shaker (Fig. 11e). Furthermore, this study has shown the generated voltage of 100 mV from the movement of a knee while operating an exercise bike when the flexible filament PEG is incorporated into a knee brace (Fig. 11f, top). Lastly, the work has demonstrated the feasibility of electrical generation from cyclic chest movement due to deep breathing. The authors show that 0.6 V is generated when the PEG is incorporated into the chest portion of a t-shirt (Fig. 11f, bottom).

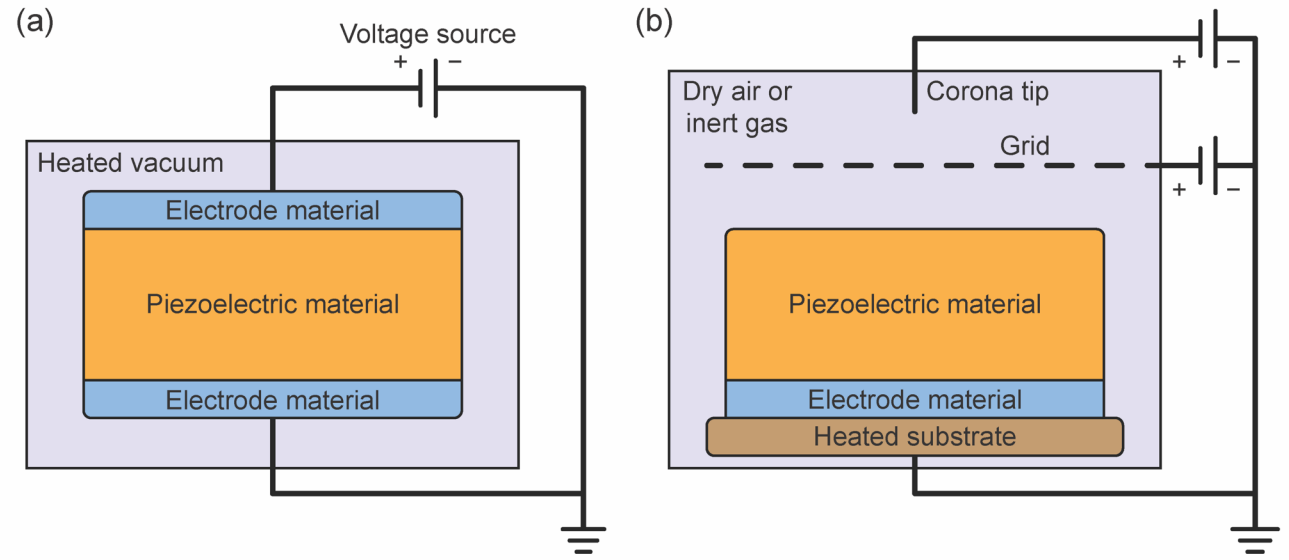

Figure 12: Schematic of poling systems for piezoelectric polymers, (a) electrode method and (b) corona poling method.

The recent advances in the deposition and processing methods for fluoropolymers show a variety of facile preparation techniques for the manufacture of PEGs. The controlled additive techniques such as 3D printing show great promise for the *in-situ* alignment of the polymer chains, preferential re-orientation into a polarized state, and potentially even electrode deposition. Furthermore, fabrication of new geometries opens up a variety of new parameters to enhance the electrical output of the flexible PEG, arising from a higher induced strain applied to each part of the PEG.

5.4. Poling techniques

The majority of deposition methods for PVDF result in a material with either a high fraction of α phase or β phase with a low degree of dipolar orientation and hence insufficient polarization vector for applications in PEGs.[43, 70, 167, 170] As a consequence, the material is required to be converted to oriented β phase to enable piezoelectric properties. Poling is a group of widely used techniques to reorient the polymer with the aim of increasing the net polarization vector in the 3 direction. Conventionally, poling is undertaken using an electric field applied along the thickness axis of the piezoelectric material at elevated temperatures.[11] The two most common methods of poling are electrode and corona techniques, which are shown schematically in Fig. 12(a and b).

Electrode poling is the least complicated method out of the two, as it only requires electrodes to be placed on both sides of the film, as shown in Fig. 12a. The system is encapsulated into an enclosure and air is evacuated from the chamber to avoid breakdown of the polymer through arcing between the electrodes.[171] Alternatively, the enclosure can be filled with an insulating fluid for the same purpose. In order to polarize the fluoropolymer material, an electric field between 5 MV m^{-1} and 100 MV m^{-1} is applied.[171, 172] Intimate contact between the polymer surfaces and the electrodes is required to achieve the desired effect of enhancing the polarization of the dipoles in the β phase of PVDF.[11]

Corona poling does not require vacuum conditions as opposed to electrode poling; however, the relative humidity needs to be minimized through circulation of dry gas, as shown in Fig. 12b. In this technique, only one electrode has intimate contact with the polymer film, allowing for the presence of patterned features on the other side.[11] The corona tip is subjected to a high voltage (10^4 V) and placed on top of a conductive grid with a much lower voltage, ionizing the gas between them and accelerating it towards the polymer, which in turn poles the material.[171, 173]

Alternative methods have been proposed to pole PVDF films into the β phase, such as electron beam poling.[174] This technique utilizes a focused electron beam, whereby the polymer is irradiated locally by electrons to overcome the energy barrier required to reorient into the β phase. This electron beam technique is quite effective at patterning small areas of material with β phase, however is not effective on a large scale.[11, 175]

The majority of flexible PEGs utilizing fluoropolymers have undertaken poling via the electrode method, with a select few opting towards the corona technique. One of the emerging trends is the deposition of electrodes onto the fluoropolymer prior to the poling, therefore using the PEGs own electrodes to pole the material.[176, 177]

Table 4 compares poling methods discussed in this review as well as their advantages and disadvantages. For scalable production of highly electroactive and efficient PVDF polymers, the poling of the polymer should be a low-energy method and be integrated as part of the deposition process, as opposed to undertaking a separate processing step to pole the material. Indeed, a topic of increasing interest in the community is the fabrication of self-poled flexible PEGs.[178-183] This type of energy harvester is able to be polarized in a single step of operation, which can arise from one of many factors, i.e., the processing

Table 4: Reported processing methods used to convert the non-polar α phase of fluorinated polymers to the electroactive β phase and pole the resultant fluoropolymer, outlining the advantages and disadvantages of each method. [11, 32, 43]

Technique	Opportunities	Limitations
Electrode poling[a)]	- High d_{33} coefficient - Reproducible	- High electric field required - Use of heat - Limited scope for structures and patterns - Undertaken in vacuum (difficult to scale up)
Corona poling[a)]	- High d_{33} coefficient - Requires only one electrode for poling - Allows for structures on one side of the material	- High voltage required - Requires heating - Undertaken in vacuum (difficult to scale up)
Electron beam poling[a)]	- Allows for patterning of highly piezoelectric regions - High resolution	- Slow and lengthy process, difficult to upscale - Unwanted chemical modification of material - Degradation of polymer - High cost process - Undertaken in vacuum
Mechanical drawing[a)]	- Highly reproducible - Simple process - Scalable	- Extrusion methods provide low scope for patterning and structuring the material - Tends to be used in conjunction with electrode or corona poling
Electrospinning	- Suitable for preparation of micro- and nano- scale fibers - Low temperature method - High degree of crystallinity can be obtained - Eliminates need for further poling	- High electric field required - Low reproducibility - Extraction of micro- and nano- fibers at low feed rates suggests low potential for scalability - Fibrous structure shows low Young's modulus and tensile properties
Additive manufacturing	- Low temperature method - High degree of crystallinity can be obtained via shear stresses at the nozzle - Scope for patterning of 3D features - Simple adaptation of designs - Reduces need for further poling	- Requires solvent-based system at low temperatures - Shortage of available literature

[a)] denotes methods commonly used for post-processing as a second step in the manufacture of electroactive fluorinated polymer

technique itself, the conditions of the deposition such as temperature, pressure and humidity, or alternatively the careful use of additives into the polymer matrix. The utilization of additives to induce preferential nucleation will be discussed in Section 5.5.

By taking advantage of electric fields (used in the electrospinning technique)[152], or shear stresses (in 3D printing), nucleation of PVDF into the electroactive phases can be achieved, showing the generation of electricity without the requirement of poling. However, of all the poling techniques, the additive technologies have recently shown the greatest promise relative to the conventional post-processing methods.

5.5. Composites, additives and nanoscale fillers

Co-polymerizing several fluorocarbon-based monomers together has demonstrated the altering of fluoropolymer properties (see Section 5.2). However, the scope for such modifications is limited. The integration of additives and nanoscale fillers into the polymer matrix has been proposed as an alternative method to achieve enhanced electromechanical properties in PVDF-based polymers. The electrical output in the resulting PEGs has been evaluated, and will be discussed in this section.

A vast range of literature exists on incorporation of fillers into the polymer matrix of PVDF and its copolymers, processed using several of the techniques outlined previously. For example, researchers have attempted to integrate piezoelectric nanoparticles (NPs), nanorods (carbon nanotubes, CNTs) and nanowires (NWs) into the PVDF matrix, showing increased electrical output due to synergetic effects between the piezoelectric NPs and the piezoelectric polymer matrix.[43] Conductive NPs, nanorods and NWs show enhanced orientation of PVDF into the desired β phase due to electrostatic interactions between the nanofiller and the surrounding polymer.[31] Furthermore, insulating and dielectric nanomaterials, such as graphene oxide and DNA, have also been shown to increase the β phase fractions of PVDF.[39, 43, 184]

Piezoelectric perovskites NPs are a primary candidate as nanofillers with the goal of increasing piezoelectric output, as they tend to show a higher piezoelectric charge coefficient (d_{33} > 100 pC N^{-1}) and a higher energy conversion efficiency (k_{33} > 0.5).[11] Indeed, the incorporation of BTO NPs with PVDF has been reported to increase the β phase fraction of the fluoropolymer matrix, scaling as a function of decreasing NP size and increasing filler content.[185] The findings suggest selective nucleation of the β phase from the BTO surface. Additionally, the formation of β

phase of PVDF is promoted by an increased surface area/volume (SA/V) ratio of the smaller particles and an increased local electric field around the BTO.[186] The maximum β fraction is determined to be 82% at a 5 wt% concentration of 10 nm diameter BTO relative to PVDF, decreasing to 70% at 10 wt% and further to 42% in 5 wt% of 500 nm BTO.[186] Recent studies have further proposed the interactions of the Ti^{4+} ion in BTO to preferentially nucleate the β phase through interactions with the fluorine atoms on the PVDF.[187]

Ferrite NPs have been added to PVDF in the form of $NiFe_2O_4$ and $CoFe_2O_4$, with an increase of β phase to 90% being reported.[188, 189] Two separate mechanisms have been previously proposed to explain the findings; (1) the epitaxial nucleation of β phase PVDF from the surfaces of the ferrite NPs and (2) the interruption of chain mobility during crystallization into the α phase which causes the polymer to crystallize into the β phase.[188] Sebastian *et al*.[190] have reported the preferential nucleation of β-PVDF in a mixture containing 1 wt% Fe_3O_4 nanorods (diameter ≈ 75 nm). This composite shows a β phase fraction of 75%, relative to 10% β phase in 1 wt% Fe_3O_4 NPs (using Eqn (19)). The authors have suggested that the increase of the β phase content is dependent upon the aspect ratio of the material. Recently, Samadi *et al*.[191] have studied the electrical output of PVDF with the incorporation of Fe_3O_4-graphene oxide hybrid nanofillers. The study shows a generated voltage of 1.75 V per N of force at 2 wt% nanofiller, whereas the pure PVDF produces 0.24 V N^{-1}.

Titanium dioxide (TiO_2) NPs with average diameter of 21 nm have been incorporated into PVDF in a solvent mixture of DMF (30 vol%) and acetone (70 vol%).[192] The study has found improved mechanical strength in the composite as well as significant increases in dielectric constant below 1 Hz (ε = 20 at 0.1 Hz compared to ε = 10 in PVDF), attributed to the increase in β phase content. It should be noted the study does not measure the β phase fraction and only postulates their findings based on the dielectric constant measurements. Lastly, the composite material shows improved strength under an applied electric field, where the breakdown voltage is 150 V μm^{-1}, compared to 50 V μm^{-1} in PVDF.

Metallic NPs have also been studied as fillers. Palladium and gold NPs integrated via solvent systems show increased β phase fractions.[193, 194] These effects have been attributed to surface charge interactions of the NPs with the dipoles of PVDF.

A variety of carbon-based nanofillers have been integrated into the matrices of fluoropolymers. The use of CNTs has been extensively studied for their effects on the formation of the crystalline β phase of PVDF, with a recent review publication on processing and characterization of composites by Kabir *et al*.[31]. More recent literature is highlighted in the following.

The incorporation of 1 wt% multi-walled CNTs (MWCNTs) has been found to increase the β fraction of PVDF from 30% to almost 50% in melt molded samples and from 0% to 40% in electrospun mats.[102] Further processing through uniaxial drawing produces β phase fractions of approximately 90% for all loadings of MWCNTs up to 1 wt%. However, the data in this study shows similar results in pure PVDF, suggesting that the effects observed here, after incorporation of CNTs, should be studied further.

The use of ultrasonication during the solution-based preparation of MWCNT/PVDF composites has been shown to induce β phase.[195] Samples are prepared via two methods, mechanical mixing (as a method with low energy input) and sonication (high energy input). The former technique produces purely α phase PVDF, while the latter technique produces predominantly β phase.[195] This phenomenon has been examined via density functional theory (DFT) calculations and is explained by the very large energy barrier required to convert the α phase PVDF to β phase.[195]

A number of studies have shown that the incorporation of ionic liquids (ILs) into the PVDF matrices is a simple method to significantly enhance the β phase fraction in PVDF. For example, Xing *et al*.[196] have used 1-butyl-3-methylimidazolium hexafluorophosphate ([Bmim][PF_6]) and MWCNTs functionalized with the same IL to make composites with PVDF. Complete conversion of PVDF to β phase has been reported in all samples containing both MWCNTs and excess amounts of IL relative to MWCNTs by weight.[196]

Maity *et al*.[197] have investigated the effects of the incorporation of IL-functionalized GO sheets into the PVDF matrix. This study reports an increase in the β phase content (through FTIR analysis and wide-angle x-ray scattering), the enthalpy of melting due to the β phase (through DSC analysis at 171.7 °C) and the mechanical properties with increasing IL-functionalized GO loading. Most of the desired metrics have shown to improve with the addition of GO; however, the study does not examine the electromechanical conversion of the resultant composite.

Dias *et al*.[198] investigated the incorporation of the IL 1-ethyl-3-methylimidazolium bis(trifluoromethylsulfonyl)imide ([Emim][TFSI]) into the matrix of PVDF at loading rates up to 40 wt%. Through the use of FTIR and Eqn. (19), the study reports improved β phase content of 93% at 25 wt% IL relative to 0% in pure PVDF. Deviating from the reports by Maity *et al*.[197], the DSC study shows a decrease in T_m from 173 °C in the PVDF to 160 °C in the 40 wt% IL/PVDF sample. This decrease can potentially be attributed to the use of IL without GO. Furthermore, the crystallinity has been reported to decrease in these samples from 44% to 25%, respectively, in agreement with the reports of Xing *et al*.[40] however opposite to the reports of Maity *et al*.[197].

In a later publication, Dias *et al*.[199] explored the same IL incorporated into PVDF for its biocompatibility with the aim of utilizing fluoropolymer-based PEGs for the purposes of implantable mechanical energy harvesting devices. In this work the authors incorporate 10 wt% IL relative to PVDF with deposition via electrospinning. Results show the lack of significant decrease in cell viability of C2C12 mouse myoblast cells on the electrospun IL/PVDF materials, suggesting that fluoropolymer-based PEGs with IL additives are biocompatible.

Recently, Lopes *et al.*[39] have used IL 1-ethyl-3-methylimidazolium tetrafluoroborate ([Emim][BF_4]) with PVDF. The study has found a linear increase in the β phase of PVDF as the IL content increases from 0% to 10%, leading to a maximum β phase content of 60%, in agreement with previous reports.[40,

[197, 198] Interestingly, by washing the composite with water at 70 °C the IL is removed from the polymer resulting in 100% β phase PVDF.[38] These findings demonstrate a low-temperature and low-energy processing pathway to the preparation of pure β phase PVDF. This study further reports a d_{33} coefficient of -27 pC N^{-1} after corona poling. The d_{33} value of the unpoled IL/PVDF system has not been measured and hence cannot be directly compared.

Fukagawa *et al*.[200] have recently investigated the piezoelectric properties of the IL [Emim][TFSI] upon incorporation into PVDF-TrFE. This study utilized a three-layer PEG, where a gel layer of 79 wt% IL in PVDF-TrFE is sandwiched between two annealed films of PVDF-TrFE, with Al electrodes on the top and bottom of the resultant structure. Through polarization switching experiments on this device, the authors report a coercive field E_C of below 10 MV m^{-1}, significantly lower than 53 MV m^{-1} obtained for the polymer without the IL. These values suggest that the required poling field strength is significantly reduced relative to pure polymer, hence decreasing the energy required to fabricate electroactive PEGs. Furthermore, the remnant polarization of this device is reported to be 64.3 mC m^{-2}, slightly lower than that of the pure PVDF-TrFE film.[200]

On the other hand, the d_{33} value for the same device is measured at 129 pC N^{-1}, increasing to 381 pC N^{-1} for a device where the active layer consists of 87 wt% IL.[200] These values are approximately an order of magnitude higher than those of a PVDF-TrFE film and hence suggest that highly efficient flexible PEGs can be fabricated from these devices.

Interestingly, Tiwari *et al*.[201] have shown the formation of the γ phase in PVDF upon the incorporation of a poly(ionic liquid), poly(2-(dimethylamino)ethyl methacrylate) methyl chloride quaternary salt. Here, the poly(ionic liquid) is added to the PVDF in solution at loadings up to 50 wt% and thin films are then solvent cast. The amount of γ phase has been reported from FTIR using Eqn. (19), where the authors justify the use of the equation by the lack of β phase (at 1275 cm^{-1}) in the sample. The fraction of the γ phase has been shown to increase from 0% in pure PVDF to approximately 50% in the sample containing 40 wt% poly(ionic liquid) in PVDF. The P-E analysis of the materials indicates a significant increase in the P_r from 14 mC m^{-2} for PVDF to 60 mC m^{-2} for the sample containing 25 wt% poly(ionic liquid). A further increase in the amount of poly(ionic liquid) results in leakage, although the P_r values are given as 62 mC m^{-2} and 66 mC m^{-2} for 30 wt% and 40 wt% poly(ionic liquid), respectively.

The utilization of ILs, due to their structure, has been suggested to aid preferential nucleation in fluoropolymers via ion-dipole interactions.[202] The effects of various ILs on the resultant crystallinity, conformation and polarization are required to be studied for greater understanding of the underlying chemistry and hence the tailoring of the electromechanical properties of these systems. Nonetheless, the current literature suggests that ILs enhance the piezoelectric properties of fluoropolymers towards efficient flexible PEGs.

Overall, the incorporation of fillers and additives in fluoropolymers shows great promise. In particular, the inclusion of nanomaterials for enhancement of electromechanical conversion is very exciting.

6. Flexible PVDF-based electric generators

PVDF is a versatile material, with properties allowing it to generate charges when mechanically deformed. Widespread efforts have been made by researchers to develop PVDF-based PEGs on both a lab scale and towards commercial applications. The following sections will discuss some of the applications of PVDF-based PEGs.

6.1. Wearable piezoelectric generators

The majority of research in fluoropolymer-based PEGs has been around applications in wearable electronics, either on-skin or as part of clothing. In fact, the first flexible polymeric PEG has been embedded in part of the shoe, allowing the wearer to generate electricity from walking.[203] Here, Kymissis *et al*.[203] have reported a shoe-embedded laminate of 16 layers of PVDF film (each 28 μm thick) bonded with epoxy, able to generate a maximum voltage and power of approximately 60 V and 20 mW per step, respectively. Due to the time-dependent nature of the electrical signal, the average power generated from this device is 1.1 mW at a frequency of approximately 1 Hz. Since then, many researchers have investigated the possibility of integrating fluoropolymers into shoe-mounted PEGs.[204-207] A comprehensive review on this topic can be found by Xin *et al*.[208].

A further mechanism for harvesting mechanical energy from human movement has been found in backpack straps. Granstrom *et al*.[209] have reported a PVDF PEG working in the 31 mode for conversion of the mechanical strain of walking with a backpack into electricity by placing PVDF into the straps. This form of PEG shows a maximum power output of 3.75 mW for a single strap with a thickness of 28 μm.[209]

More recently, PEGs integrated into textiles have become a topic of great interest. A variety of publications have proposed the use of fluoropolymer fibers in woven textiles utilizing electrospinning and mechanical drawing techniques.[210-214] The fabrication of PVDF fibers towards utilization in energy harvesting textiles has been initially reported by Hadimani *et al*.[215]. This study shows a maximum generated voltage of 2 V when a 1.02 kg mass is dropped from a height of 5 cm onto several fibers sandwiched between two copper plates, indicating prospects for the use of PVDF fibers as a textile PEG.

Magniez *et al*.[216] have presented initial reports on 2D woven PVDF textile generators using melt-extruded and drawn piezoelectric fibers, along with silver-coated nylon fibrous electrodes and non-conductive nylon as a spacer, shown in Fig. 13a. This 2D woven device has an average voltage between 3 V and 4 V, with a maximum of 6 V under cyclic compression with a force of 70 N (shown in Fig. 13b). In another study, the group has analyzed the impacts of the electrode materials on the output voltage, finding that silver-coated copper electrodes show the highest generated voltage under sine wave shaped

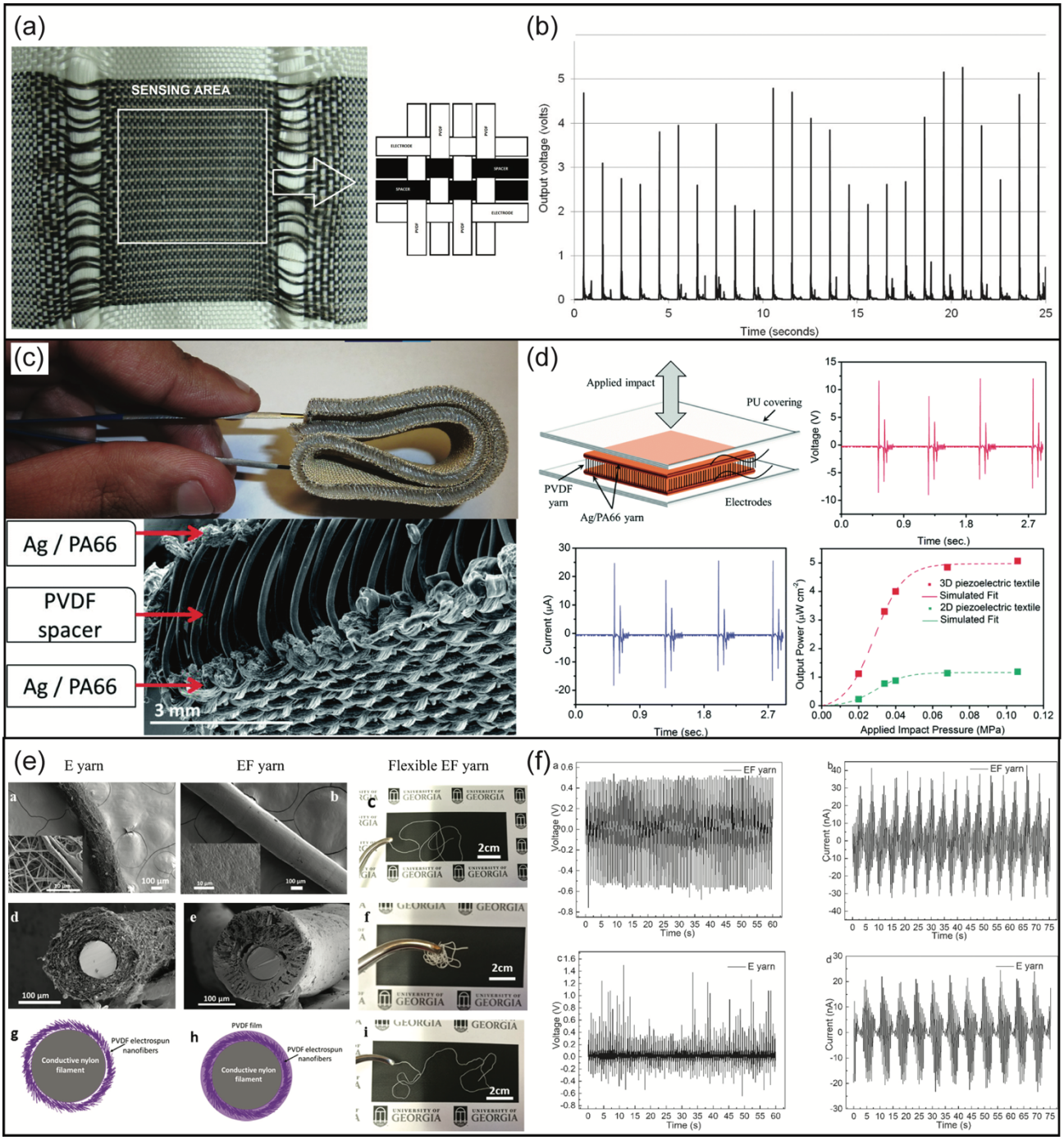

Figure 13: The morphological structure and electrical output characteristics of recently reported woven fluoropolymer flexible PEGs. (a) the woven flexible PVDF fabric PEG with a schematic of the weave pattern on the right and (b) the voltage generated from the PEG upon cyclic compression. Reproduced with permission from ref 216. Copyright 2013, Wiley. (c) image (top) demonstrating the flexibility of the PVDF-based 3D spacer textile PEG, cross-sectional SEM image (bottom) of the PEG, and (d) the electrical output characteristics including the voltage, current and power of the PEG under cyclic compression. Reproduced with permission from ref 30. Copyright 2014, Royal Society of Chemistry. (e) SEM images of the electrospun (E) and electrospun + film core-sheath (EF) yarns, with a schematic outlining the cross-sectional view, with optical images of the yarns. (f) output characteristics including the voltage and current from the EF yarn (top) and E yarn (bottom) under cyclic compression. Reproduced with permission from ref 219. Copyright 2018, Institute of Physics.

vibration. Here, the work has analyzed metal-wire electrodes consisting entirely of aluminum, titanium or steel, as well as coaxial fibers composed of either nylon or copper core with a silver coating external layer. It is noted that the various materials used in the study are not consistent in their geometry and hence are difficult to compare directly.[217]

The work of Soin *et al.*[30] has demonstrated a 3D spacer textile, woven using silver-coated polyamide-66 (PA66) yarn as electrodes, with melt-spun and poled PVDF fibers as the piezoelectric yarn between them, shown in Fig. 13c. This PA66-PVDF-PA66 system, which feels just like standard fabric, is able to generate a voltage up to approximately 14 V, with a power

density of 5.10 μW cm^{-2} at an impact pressure of 0.1 MPa (Fig. 13d). Similarly, Talbourdet *et al*.[218] have reported on a 3D interlocked woven PVDF textile, generating a maximum voltage of 2.3 V (average 1.29 V) with an overall energy of 10.5 μJ m^{-2} (at a resistance of 1 MΩ). These values have been achieved through cyclic compression of the textile at a frequency of 100 Hz and a force of 5 N. The authors have reported a power output density on the order of 10^{-12} W cm^{-2}, significantly lower than the values reported in the work of Soin *et al*.[30]. It should be noted that in this study the electrodes are not woven into the textile; instead, bulk copper electrodes are used, which results in measured voltage losses upon decompression. All of the aforementioned PVDF-based textile PEGs have utilized melt-spinning to obtain fibers, with mechanical drawing and dual-electrode electrical poling of the fibers used during spinning to increase the amount of β phase and polarization within the fibers, respectively.

More recently, Gao *et al*.[219] have produced a piezoelectric yarn by electrospinning of a PVDF solution onto a silver-coated nylon yarn, followed by coating with PVDF by passing the resultant yarn through a solution of PVDF to produce an electrospun + film core-sheath yarn (Fig. 13e). An external silver electrode has been deposited onto the outer surface of the yarn via electron beam evaporation. A single yarn with a length of 3 cm has been reported to produce a voltage and current of 0.52 V and 18.76 nA, respectively (Fig. 13f). The volumetric power density has been reported as 5.54 μW cm^{-3} when exposed to cyclic compressions at 0.02 MPa pressure at a frequency of 1.85 Hz.

Similarly, Lund *et al*.[29] have fabricated a coaxial fiber PEG, which has been woven via plain weave and twill patterns into a textile. This work has used a melt-spinning mechanism to simultaneously co-extrude a fiber with a conductive core consisting of 10 wt% carbon black in polyethylene and an outer piezoelectric layer consisting of PVDF. Polyamide yarns coated with Ag have been utilized as the outer electrodes. To demonstrate the applicability of these flexible PEG textiles, they have been incorporated into the shoulder strap of a bag. During walking, with the strap carried by hand, the PEG is reported to generate 1.9 μW cm^{-3} volumetric power density. This power density is notably lower than the work of Gao *et al*.[219], even though this report has poled the material via the corona method. This type of PEG has additionally been shown to provide enough electrical energy to power a commercial LED after 15 sec of charging a 22 μF capacitor, resulting in continuous blinking of the LED with an average frequency of 0.13 Hz.

PVDF-based flexible yarn PEGs certainly have been shown to have the potential to be woven into textiles for the scavenging of energy from human movements into electricity. Furthermore, the proof-of-concept textile PEGs mentioned in this section show the potential of transformation into industrial products such as smart clothing with the ability to power portable electronic devices in a sustainable manner, through the scavenging of the wearer's movements.

6.2. Implanted piezoelectric generators

Another promising use of fluoropolymer-based flexible PEGs is harvesting biomechanical energy to power implantable electronic devices, such as permanent pacemakers, implantable cardioverter-defibrillators, cardiac resynchronization therapy devices, and long-term implantable wireless sensors among others. The main drawback of current generation devices lies in the lifespan of the batteries; consequently, implanted devices are required to be removed from the body for the replacement of their power sources. Thus, using flexible PEGs to harvest biomechanical energy can be advantageous for the purposes of powering such devices, as has been reported recently by several authors.[220-224]

The first reports of an implanted fluoropolymer PEG have been published by Hausler *et al*.[225]. This study investigates the *in-vivo* operation of a PEG, with PVDF as the active material, attached to a rib of a dog in order to harvest energy from respiration. The *in-vivo* experiments have shown a maximum voltage of 18 V, corresponding to a power of 17 μW, with no loss in durability over the three hours of the experiment.

Cheng *et al*.[226] have fabricated an implantable self-powered PVDF blood pressure sensor, based on the principles of PEGs (Fig. 14a). This device has been found to generate a maximum instantaneous power of 2.3 μW during *in-vitro* experiments, whereby the thin film PEG is wrapped around a tubular latex artery analogue filled with saline (Fig. 14b). Here, the deformation is induced using an intra-aortic balloon pump to mimic the pumping action of the heart. The *in-vivo* studies in this work have been found to generate a maximum instantaneous power output of 40 nW with the device wrapped around the aorta of a Yorkshire porcine (Fig. 14c). Here, the generated power is found to scale linearly with systolic blood pressure, whereby the maximum is obtained at 220 mmHg. Although no voltage or power data has been presented for blood pressure below 160 mmHg, the study further reports a liquid crystal display to be powered directly by the cyclic expansion and contraction of the aorta at blood pressures at, and above, 140 mmHg with no additional electrical signal conditioning or electrical energy storage connected (Fig. 14a).

Yu *et al*.[227] have reported an implanted sponge-like PVDF-based thin film PEG (Fig. 14d) inserted under the skin of living mice and rats. During *in-vitro* testing of the PEG in the mode of cantilever-like deflection under an applied strain of approximately 0.1%, the device has been found to generate a maximum voltage and current of 3.8 V and 3.5 μA, respectively, corresponding to an instantaneous power of 13.3 μW (Fig. 14e). The PEG has been further inserted beneath the skin of the right leg of a mouse and its electrical output has been measured during manual deflection of the leg (Fig. 14f). Similar to the work of Cheng *et al*.[226] discussed above, both the voltage and current, 0.26 V and 0.17 μA, respectively, are lower than during *in-vitro* tests, corresponding to 44.2 nW instantaneous power (Fig. 14f). Although it is difficult to directly compare the two studies, the values of the maximum instantaneous power generated are similar. Of note is the biocompatibility study performed in the work of Yu *et al*.[227], which suggests no signs of toxicity or incompatibility under the skin of the mice after six weeks. As a proof-of-concept, this study demonstrates the utilization of a

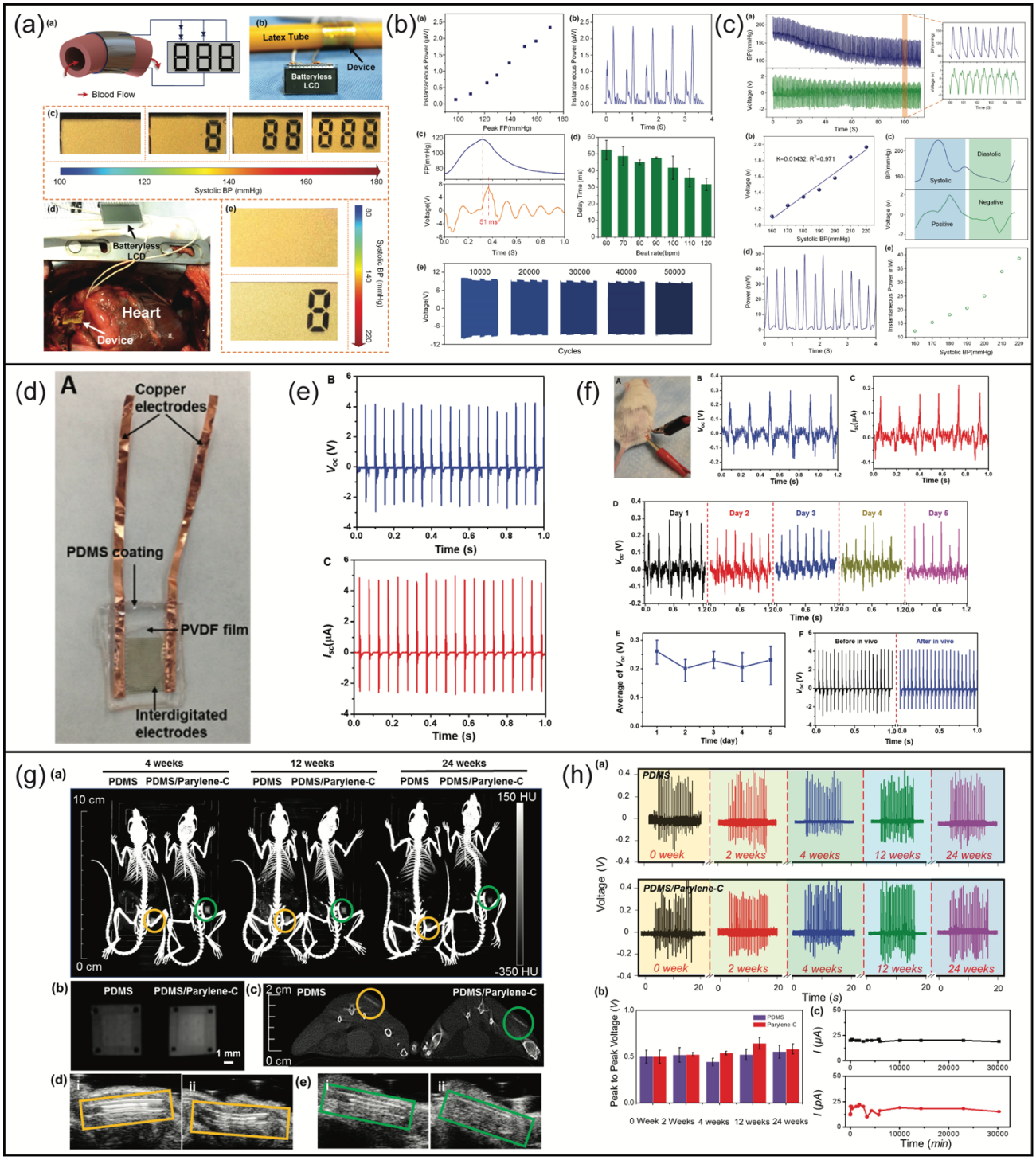

Figure 14: The structure and electrical output characteristics of recently reported implanted fluoropolymer flexible PEGs. (a) Schematic (top) showing the working conditions for the implantable PEG and (bottom) implanted fluoropolymer PEG wrapped around the aorta of a Yorkshire porcine, both showing the ability to power a battery-less LCD display above a blood pressure of 120 mmHg *in-vitro* and 140 mmHg *in-vivo*. (b) The electrical output characteristics of the *in-vitro* experiment when wrapped around a latex tube mimicking the aortic artery and (c) the electrical output characteristics of the *in-vivo* experiments. Reproduced with permission from ref 226. Copyright 2016, Elsevier. (d) Image showing the structure of the implantable fluoropolymer PEG encapsulated in poly(dimethyl siloxane), (e) the electrical output characteristics during *in-vitro* experiments, showing the open circuit voltage and short circuit current, and (f) electrical output characteristics during the *in-vivo* experiment, showing the image of the PEG implanted in a mouse, the open circuit voltage and short circuit current when the leg of the mouse is deflected manually, as well as the output of the PEG as a function of implanted time. The bottom-right panel shows the *in-vitro* open circuit voltage before and after implantation. Reproduced with permission from ref 227. Copyright 2016, Elsevier. (g) In-vivo computed tomography images (top) of the PVDF PEGs encapsulated in poly(dimethyl siloxane) and Parylene-C during the implantation period, as well as ultrasound images of the devices implanted in mice. (h) Electrical output characteristics of the long-term implanted PVDF PEGs, showing (top) the voltage of both devices, (bottom left) average peak-to-peak voltage as a function of implantation period for both devices and (bottom right) the input and output currents durind characterization of the leakage current in the device encapsulated in poly(dimethyl siloxane) as a function of time. Reproduced with permission from ref 228. Copyright 2016, Elsevier.

miniaturized energy storage package attached externally to the back of the mouse (in a backpack-like manner), consisting of a rectification circuit and a 1 μF capacitor, able to store the harvested electricity from the implanted PEG, with a steady open circuit voltage of 0.052 V.

More recently, Li *et al*.[228] has undertaken a follow-up study on the long-term *in-vivo* biocompatibility of a PVDF-based PEG. Their research examines the safety of encapsulated PVDF-based PEGs under *in-vivo* conditions for up to six months post-implantation, namely for the presence of inflammatory infiltration, fibrosis, muscle degeneration and cellular anomalies (Fig. 14g).[228] Additionally, the electrical output of the PEGs has been studied *in-vitro*, after the implantation for up to six months (Fig. 14h). In this set of experiments, each device has been initially implanted into a mouse for a set period and extracted for *in-vitro* tests.

This extensive study has shown that the implantation of fluoropolymer-based PEGs does not show signs of cytotoxicity *in-vivo* throughout long-term implantation. Relative to the previous study by Yu *et al*.[227] (same group), this study reports a lower *in-vitro* electrical power value of 13.5 nW, based on 0.3 V potential difference and 45 nA current (when the PEG is deflected by an electromagnetic shaker with a force of 6 N and a frequency of 2 Hz). However, we note that a different frequency has been applied between the two studies, which makes it difficult to compare the relevant results. Similar to the previous study,[116] the voltage generation of the PEG has been tested *in-vivo* through stretching of the leg muscle of the mouse, as the PEG has been implanted subcutaneously onto the leg muscle.[117] A peak-to-peak voltage of 0.05 V at a leg-stretching frequency of 1 Hz and 0.1 V at 2 Hz has been reported. Lastly, the implanted PEGs removed from the mice after six months for voltage testing show no long-term degradation of piezoelectric properties due to implantation of the device.[117]

These studies have been the first to provide insights into the stability and durability of fluoropolymer-based PEGs in the body, suggesting their suitability for commercial applications in the field of powering implanted electronic devices. In the current state of the field, more work needs be undertaken on *in-vivo* studies and utilizing more powerful fluoropolymer PEG systems reported elsewhere. We fully expect that fluoropolymer PEGs will contribute significantly to future applications in the healthcare sector.

6.3. Piezoelectric generators driven by the environment

Harvesting energy from the urban and natural environments (external mechanical stimuli such as road deformation under passing vehicles, vibration, wind and water flow) has been previously shown as a viable option for building sustainable electricity generators towards reducing the reliance on fossil fuels. Of these, wind-based energy harvesting has seen the greatest commercial acceptance.

External mechanical forces are present and abundant throughout the environment, implying that energy harvesters based on the principles of piezoelectricity are suitable candidates to generate electricity from these sources. A variety of innovative applications have been both proposed and validated at a laboratory scale. Among these, is the harvesting of mechanical energy from the movement of vehicles on a road, previously proposed as one of the technologies enabling "smart roads".[22, 229, 230] PEGs are anticipated to be capable of powering street lamps and nearby buildings, in addition to acting as sensors for monitoring the ongoing traffic density and the condition of the road itself.[231] Employing PEGs as sensors is forecasted to optimize traffic signal timing for the reduction of roadway congestion and to assist in the efficient allocation of road maintenance resources.[232]

Initially, piezoelectric ceramic materials have been utilized for this purpose and have shown significant promise. In fact, attempts have been made to commercialize this technology using PZT as the active piezoelectric component, and pilot-scale studies to validate the viability of the roadway PEGs have been undertaken.[233]

For efficient and long-term use of this technology, flexible materials are highly desirable to prevent cracking when integrated under the pavement surface of the road. In this instance, polymeric materials with a much lower Young's modulus are more suitable relative to their brittle, ceramic counterparts. The first report of a PEG, with PVDF as the active material, embedded into a road is from Jung *et al*.[22], shown in Fig. 15(a-c). This study utilized a commercial PVDF film with a thickness of 110 μm to create laminated stacks of up to 60 piezoelectric films with an optimized initial radius of curvature for use in the 31 mode of operation. Each harvester in this study consists of two PVDF films immobilized on the front and back sides of a polyimide substrate (300 μm thickness, predetermined radius of curvature) by using nickel-based fabric tape, which acts as the electrode (Fig. 15a). The electrical output for the unit harvester has been reported to result in an open circuit voltage of 61.2 V and a short circuit current of 18.4 μA under a strain rate of 1.5% s^{-1}.[22]

Through optimization of the initial radius of curvature to 300 mm, the study has claimed an increase in the open circuit voltage of 75 V, justified by an increase in the maximum induced stress. A set of ten unit harvesters have been connected in parallel, and consequently attached to a suitable resistor via a rectifying bridge. Under similar strain conditions, this set has been reported to output 3.6 mW, corresponding to 38 V and 96.8 μA at the impedance-matched resistive load of 400 kΩ (Fig. 15b).[22] Jung *et al*.[22] have further investigated the energy harvesting characteristics of a PEG consisting of six sets of harvesters, with a total of 60 unit harvesters (or 120 PVDF thin films) in parallel, which is tested under a simulated load of a passing vehicle (using a model mobile load simulator, shown in Fig. 15c). The reported maximum instantaneous power output due to the equivalent of a personal vehicle moving at 8 km h^{-1} (with a reported force of 2.5 kN) is 200 mW, corresponding to 88.9 V and 2.25 mA at an impedance-matched resistance of 40 kΩ (Fig. 15c). The authors have further claimed a calculated power density of 8.9 W m^{-2} for the roadway PEG, acceptable for large-scale energy harvesting under the pavement in roads.

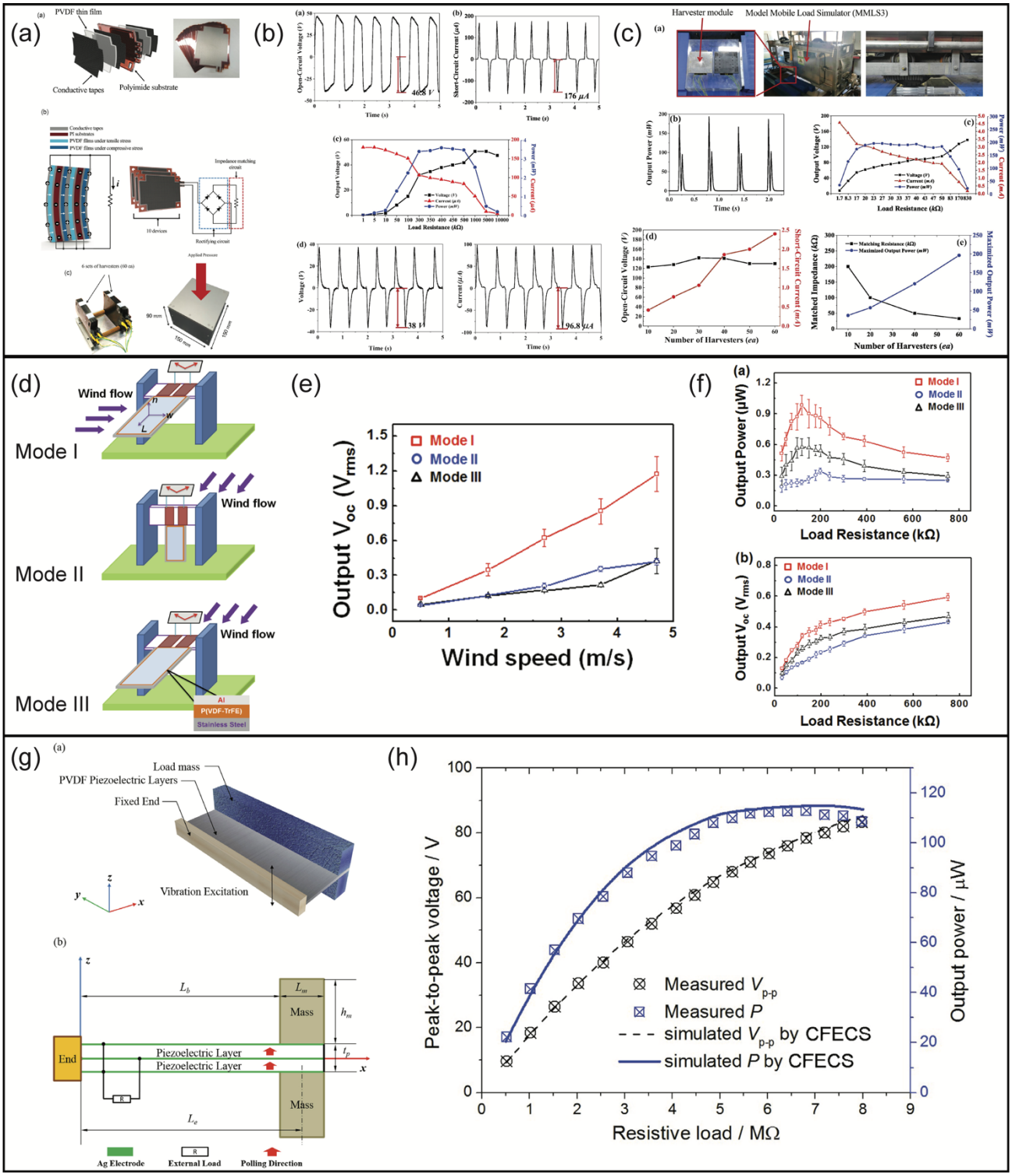

Figure 15: The structure and electrical output characteristics of recently reported environment-driven fluoropolymer flexible PEGs. (a) Schematic and images showing the contents of the roadway unit harvester, as well as the ten-unit systems and 60 unit systems studied in this report. (b) The electrical output characteristics of the ten-unit systems, showing (top) V_{OC} and short circuit current, (middle) the resistance matching data, and (bottom) the voltage and current at the matched load resistance of 400 kΩ. (c) The electrical output characteristics of the 60-unit systems under simulated road conditions, showing (top) images of the experiments, (middle) resistance matching data and power across a 400 kΩ resistor and (bottom) V_{OC} and short circuit current as a function of the number of unit harvesters, as well as the matched load resistance and power output of the road-harvesting PEG as a function of the number of unit harvesters. Reproduced with permission from ref 22. Copyright 2017, Elsevier. (d) Schematic showing various geometries tested for the PVDF wind-harvesting PEG, (e) generated V_{OC} as a function of wind speed for the three geometries and (f) resistance matching data showing (top) the output power and (bottom) V_{OC} as a function of load resistance. Reproduced with permission from ref 238. Copyright 2014, American Institute of Physics. (g) Schematic showing the structure of the optimized vibration-excited PVDF PEG and (h) electrical output characteristics at an optimized of 34.4 Hz as a function of load resistance, based on simulated optimized geometry. Reproduced with permission from ref 131. Copyright 239, Elsevier.

An alternative approach has recently been proposed for harvesting energy in high-speed railway applications.[234] This technique utilizes PVDF films acting as cantilevers placed inside Helmholtz resonators to harvest energy from the vibrations induced by moving trains, while providing a secondary function as a noise-reducing barrier. At the experimentally-optimized resonant frequency of 447 Hz and impedance-matched resistance of 6 kΩ, the PVDF film PEG (thickness = 200 μm) has been reported to produce a maximum power of 1.24 μW, corresponding to a voltage and current of 74.6 mV and 16.6 μA, respectively. This value is obtained at a sound pressure level of 110 dB. Interestingly, the power output noticeably decreases to 0.59 μW (52.2 mV, 11.3 μA) when the sound pressure level dropped to 100 dB. This is an interesting innovative application for flexible PEGs and this group appears to be progressing towards large-scale installations consisting of 480 Helmholtz resonator PEG devices per module.

The harvesting of energy from natural environments using flexible PVDF-based PEGs has also been previously reported. For example, Vatansever *et al*.[235] have fabricated a PVDF cantilever PEG, with half of the length secured to the support and the other half suspended in air. This study investigates the ability of the PEG to generate electricity from falling raindrops and wind under dynamic conditions. Two lengths of 28 μm thick PVDF film were used for the experiment, 41 mm and 171 mm, each sandwiched between two Cu-coated polyester laminates. The raindrop experiment has reported that the 41 mm-long PVDF PEG generates an open circuit voltage of approximately 2.3 V when a droplet weighing 7.5 mg is dropped from a releasing height of 100 cm, increasing to approximately 12 V for a droplet weighing 50 mg.[121] Furthermore, the authors report the open circuit voltage of a short PVDF cantilever PEG to be significantly higher than that of a composite consisting of uniaxially aligned PZT fibers in an epoxy matrix under similar experimental conditions.[121]

Vatansever *et al*.[235] have further characterized the power generated for the aforementioned flexible cantilever-type PVDF PEGs, suggesting that the short PVDF strip generates an electrical power on the order of nanowatts, whereas the longer sample generates 93.6 μW at a wind speed of 10 m s^{-1}. Comparatively, the same study has reported a PZT composite, generating 6.5 μW for a single layer PEG and 3.6 μW for a bimorph.[235] The authors further reported a volumetric power density of 16.2 μW cm^{-3} at 5 m s^{-1} and 157.9 μW cm^{-3} at 10 m s^{-1} wind speed, the latter showing an increase over the PZT composite by a factor of 16.

Work by Li *et al*.[236] has investigated the effects on the positioning of a flexible cantilever-type PVDF wind-driven PEG relative to the direction of the wind and correlating it to the electrical generation capability. Two directions have been investigated, using a parallel-flow device and a cross-flow device, positioned parallel and perpendicular to the wind flow direction, respectively. The study reported an enhanced power density from the cross-flow device relative to the parallel-flow device, with maximum values of approximately 14 μW and 3.5 μW, respectively, at a wind speed of 6.5 m s^{-1} and a load resistance of 1 MΩ. Increasing the load resistance to 10 MΩ, the maximum power output increases to 296 μW in the cross-flow device at a wind speed of 8 m s^{-1}. The maximum volumetric power density at a moderate wind speed of 5 m s^{-1} has been reported at 68.5 μW cm^{-3}.

Further work by the same research group has investigated similar PEGs with varying dimensions, the long cantilever (72 mm length and 16 mm width), the short cantilever (41 mm length and 16 mm width) and a narrow short cantilever (41 mm length and 8 mm width).[237] The varying devices have been immobilized in a wind tunnel with cross-sectional dimensions of 25 cm in height and 25 cm in width in the cross-flow orientation, whereby the induced wind speed ranged from 0 m s^{-1} to 8 m s^{-1}. The generated volumetric power density has been investigated with varying wind speed, showing that the long cantilever-type PEG has the highest values at wind speeds below 4 m s^{-1}. Results also indicate that the narrow short cantilever-type PEG generates the highest power densities between 4 m s^{-1} and 7.5 m s^{-1}, whereas at 8 m s^{-1} the short cantilever generates the highest volumetric power density at approximately 1.5 mW cm^{-3}.[123] The study further reports that a maximum generated volumetric power density of 2.0 mW cm^{-3} is obtained for the narrow short cantilever with a load resistance of 30 MΩ. However, no data is shown for the influence of the variation of load resistance on the electrical output of the wind-powered PEGs.

Li *et al*.[238] have utilized a PVDF-TrFE copolymer thin film as the piezoelectric layer in flexible wind-powered PEGs and have investigated the electricity generated from three geometries, shown in Fig. 15(d-f). Mode I and mode III correspond to cross-flow and parallel-flow devices as outlined above, whereas mode II corresponds to the wind flow perpendicular to the PEG in a manner where the wind impacts the surface of the PEG (Fig. 15d). In this work, the PVDF-TrFE layer has a thickness of 4 μm and is deposited onto an 8 μm thick stainless steel foil acting as the bottom electrode. The resulting structure is then annealed at 130 °C for 2 h. The top electrode consists of a 100 nm thermally evaporated layer of Al, and post-processing is undertaken to polarize the piezoelectric layer. This work, compared to the aforementioned studies, has investigated wind speeds below 4.7 m s^{-1}, as those speeds are more comparable to those found in nature. However, the wind tunnel in Li *et al's*[238] study has a circular cross-section with a diameter of 8.5 cm. The comparative study of the three modes suggests a linear increase in the generated open circuit voltage as a function of wind speed, whereby the cross-flow (mode I) device shows the highest open circuit voltage of the investigated harvesting modes at approximately 1.2 V (Fig. 15e). This is four times higher than those of modes II and III. Through resistance matching experiments at a wind flow of 3.9 m s^{-1}, the output power for the mode I device has been reported as 0.98 μW for a resistive load of 120 kΩ (Fig. 15f). This value corresponds to a volumetric power density of 233 μW cm^{-3} based on top electrode dimensions of 7 cm length and 1.5 cm width. This value is lower than the previously reported volumetric power output; however, it should be noted that differences in design could have contributed to the changes in output values.

More recently, Song *et al*.[239] have investigated a generalized case of off-resonance vibration-based excitation of a flexible PVDF bimorph PEG in the shape of a cantilever with a fixed mass at the end (Fig. 15g). The work utilizes a coupled finite-element-circuit approach to optimize the parameters of the PEG, and the results of modelling are verified in experimental studies. The maximum volumetric power density for two 50 μm thick PVDF layers bonded together with thin Ag electrodes has been reported as 8.61 mW cm^{-3} with an optimized load resistance of 6.81 MΩ (Fig. 15h). The excitation acceleration has been reported as 0.5 g at the optimized frequency at 34.4 Hz, corresponding to 25.5 MPa maximum stress.

These examples are intended to provide an overview of the possible applications where flexible polymeric PEGs have been previously utilized. These promising proof-of-concept devices are expected to encourage further growth of prospective applications in this field, both in laboratories and in commercial settings.

7. Concluding remarks and future perspectives

Flexible fluoropolymer-based PEGs have attracted increasing attention as a promising energy harvesting solution due to their mechanical flexibility, transparency, operating temperatures suitable for widespread use, high compatibility with straightforward deposition and processing methods, biocompatibility and high piezoelectric energy conversion efficiencies. This type of PEGs has been demonstrated for applicability in either directly powering a range of electronic devices or providing an additional source of electricity for their operation. This all assists in decreasing the reliance on the outdated conventional electricity generation and storage technologies.

Despite the advancement of flexible PEGs in the recent years, challenges remain before the commercial adoption of these devices can occur. These challenges arise largely from a lack of clear understanding of the connection between the various aspects of this complex field. Currently, the field appears heavily segmented into largely independent studies undertaken by polymer chemists exploring novel synthetic routes, and material scientists and engineers processing and depositing the polymers into useful devices, with mechanical engineers optimizing the physical parameters for enhanced energy conversion, and electrical engineers efficiently integrating the PEG into usable devices. It is therefore, important that these fields work together to successfully produce devices with the required parameters to maximize the energy conversion from mechanical force to electricity and the production of commercially relevant devices.

Moreover, the characterization techniques utilized by each of these disciplines, generally, do not provide a complete description of the flexible fluoropolymer PEG systems, reducing the ability to directly and quantitatively compare the results obtained. Therefore, the development of cross-disciplinary collaborations between the disciplines holds great potential in facilitating the in-depth understanding of complex connections between the chemistry of fluoropolymers, their processing, and the properties of the resulting flexible PEGs.

Aside from the shift towards multidisciplinary studies, optimizations of the current methods in each discipline is also crucial. For example, the current spectroscopic techniques used to fingerprint the phases of PVDF, and related polymers, show clear limitations. The FTIR technique, commonly used in the characterization of these polymers, often results in complex spectra with overlapping peaks for the β and γ phases. Recent literature has attempted to overcome this constraint; however, further efforts are required. The utilization of Raman spectroscopy leads to characteristic peaks for the various phases with higher resolution relative to FTIR; however, is currently underutilized in literature. Simultaneous DSC-Raman can also provide a fingerprint both of the relative phase content and the overall crystallinity.

Additionally, the currently accepted methods for measuring the net polarization vector are limited in their scope—the P-E hysteresis technique utilizes an electric field which has the parasitic effect of poling the material and therefore generally provides only the maximum polarization that can be obtained in the fluoropolymer. Characterizing the net polarization within the sample without affecting it will provide insight into the net dipole vector in the fluoropolymers without influencing the system. We strongly encourage the researchers within this field to pay appropriate attention to developing a suitable characterization method for polarization measurements.

Currently, poling is commonly used as an additional step to polarize the fluoropolymers in PEGs; however, as we discuss in Section 5.4, this step is undesirable because it utilizes high temperature and high electric fields. Therefore, methods to produce suitable fluoropolymers for PEGs without poling are extremely interesting. It is very exciting that scalable solvent-assisted extrusion technologies such as 3D printing and electrospinning have been recently shown to be able to provide *in-situ* poling (without the need for the post-processing via electric fields) through either shear stresses or induced electric fields, respectively. The ability to fabricate flexible PEGs in a shorter number of fabrication steps and with less energy input is expected to be a key contributor in driving the commercialization of the PEG and further increase the prospects of sustainable energy harvesting methods.

The emergence of additive manufacturing technologies such as 3D printing and electrospinning has opened the door for advanced fluoropolymer structures, which have been difficult to explore previously. In particular, preliminary research in the fabrication of high aspect ratio structures has reported drastic improvements in the energy conversion efficiency of fluoropolymers. It is our expectation that various new 3D printing technologies, such as fused deposition modeling, solvent-evaporation assisted printing and melt electrowriting (among others), will enable layer-by-layer and true 3D extrusion of the fluoropolymers and lead to the increase of energy conversion efficiency in flexible PEGs. In addition, multi-material printing shows great potential for complete end-to-end production of PEGs through the controlled deposition of

electrode materials, reducing waste and providing a true single-step fabrication technique.

Another exciting developing area to emphasize is the incorporation of additives into piezoelectric fluoropolymers. Preferential reorientation of the crystalline phases of the polymer into the β phase has been proposed as the standard mechanism of increasing the electromechanical conversion, due to either steric or electrostatic interactions. However, the optimization of crystallinity and polarization using additives has not been systematically explored to date. These factors influence the electrical output from electromechanical conversion in flexible PEGs and hence it will be critical to investigate the influences and the underlying mechanisms of nanomaterials and other additives on the enhancement of these properties.

In general, the new developments in understanding how the properties of fluoropolymers enable future flexible PEG applications has led to a significant push in research efforts in recent years. Future fluoropolymer-based PEG research is anticipated to provide further insights into the understanding of the open questions posed in this review. Several key open questions remain unanswered, some of which are as follows: (1) the literature on process-dependent polarization enhancement is currently limited in its scope, attributing enhancements of energy conversion efficiency to increases in either the β phase or the total polymer crystallinity. The understanding of how processing techniques affect (and more importantly enhance) the polarization is critical to progressing the field; (2) there is large scope to move away from electrical fields for poling to enhance polarization to study shear-induced polarization through various techniques such as 3D printing; (3) there needs to be a stronger fundamental understanding of how the properties of the fluoropolymers influence the electrical output which ties into fully characterizing the materials and not just focusing on single properties of the material such as β phase or output, as this is a multi-parametric system; (4) the use of non-destructive techniques are expected to provide new and valuable information such as confocal Raman microscopy, piezoresponse force microscopy (PFM) and 3D magnetic resonance imaging (MRI), among others.

The future for low-energy, always-on electronic devices and wireless sensors is emerging fast. Flexible polymeric PEGs have great potential in these devices and pose a unique opportunity for the sustainable energy harvesting from mechanical energy, which is abundant in daily life. This type of energy harvesting will act to reduce the reliance on powering electronic devices from the grid, opening up new possibilities for personal and wearable electronics, as well as long-term implantable medical diagnostics and cardiac devices. We are expecting to see more and more inspirational developments in the applications of flexible fluoropolymer PEGs in the near future.

Conflicts of interest

There are no conflicts to declare.

Acknowledgements

This research was supported by the Australian Government through the Australian Research Council's Linkage Projects funding scheme (LP160100071) and Future Fellowships funding scheme (FT130100211).

References

1. Z. L. Wang, G. Zhu, Y. Yang, S. H. Wang and C. F. Pan, *Mater. Today*, 2012, **15**, 532-543.
2. P. Satyavolu, S. J. Cherian and S. Rajagopalan, *Wearable Technology: Automotive's Next Digital Frontier*, Cognizant, 2015.
3. Y. F. Zheng, J. Huang, G. Wang, J. M. Kong, D. Huang, M. M. Beromi, N. Hazari, A. D. Taylor and J. S. Yu, *Mater. Today*, 2018, **21**, 79-87.
4. X. Y. Peng, T. W. Root and C. T. Maravelias, *Green Chem.*, 2017, **19**, 2427-2438.
5. Clean Energy Council, *Clean Energy Australia Report 2018*, 2018.
6. E. Fatuzzo, H. Kiess and R. Nitsche, *J. Appl. Phys*, 1966, **37**, 510-&.
7. C. R. Bowen, J. Taylor, E. LeBoulbar, D. Zabek, A. Chauhan and R. Vaish, *Energy Environ. Sci.*, 2014, **7**, 3836-3856.
8. H. Ohigashi and K. Koga, *Jpn. J. Appl. Phys., Part 2*, 1982, **21**, L455-L457.
9. K. Koga and H. Ohigashi, *J. Appl. Phys*, 1986, **59**, 2142-2150.
10. C. Jean-Mistral, S. Basrour and J. J. Chaillout, *Smart Mater. Struct.*, 2010, **19**, 14.
11. K. S. Ramadan, D. Sameoto and S. Evoy, *Smart Mater. Struct.*, 2014, **23**, 033001-033026.
12. J. Curie and P. Curie, *Bull. soc. min. de France*, 1880, **3**, 90-93.
13. J. Curie and P. Curie, *Comptes Rendus*, 1881, **93**, 1137-1140.
14. M. G. Lippmann, *Philos. Mag.*, 1881, **12**, 151-154.
15. *US Pat.,* 1495429, 1924.
16. *US Pat.,* 1864638, 1932.
17. *US Pat.,* 2248870, 1941.
18. *US Pat.,* 3239678, 1966.
19. S. Jana, S. Garain, S. Sen and D. Mandal, *Phys. Chem. Chem. Phys.*, 2015, **17**, 17429-17436.
20. Y. Imai, D. Tadaki, T. Ma, Y. Kimura, A. Hirano-Iwata and M. Niwano, *Sens. Actuators, B*, 2017, **247**, 479-489.
21. X. L. Chen, X. M. Li, J. Y. Shao, N. L. An, H. M. Tian, C. Wang, T. Y. Han, L. Wang and B. H. Lu, *Small*, 2017, **13**, 1604245.
22. I. Jung, Y. H. Shin, S. Kim, J. Y. Choi and C. Y. Kang, *Appl. Energy*, 2017, **197**, 222-229.
23. B. Saravanakumar, S. Soyoon and S. J. Kim, *ACS Appl. Mater. Interfaces*, 2014, **6**, 13716-13723.
24. Y. L. Zi, L. Lin, J. Wang, S. H. Wang, J. Chen, X. Fan, P. K. Yang, F. Yi and Z. L. Wang, *Adv. Mater.*, 2015, **27**, 2340-2347.
25. P. Dineva, D. Gross, R. Muller and T. Rangelov, in *Dynamic Fracture of Piezoelectric Materials*, Springer, Dordrecht, 2014, vol. 212, pp. 7-32.
26. W. Voigt, *Lehrbuch der kristallphysik (mit ausschluss der kristalloptik)*, Springer-Verlag, 1910.
27. A. S. Bhalla, R. Y. Guo and R. Roy, *Mater. Res. Innov.*, 2000, **4**, 3-26.

28. D. Y. Park, D. J. Joe, D. H. Kim, H. Park, J. H. Han, C. K. Jeong, H. Park, J. G. Park, B. Joung and K. J. Lee, *Adv. Mater.*, 2017, **29**, 1702308.
29. A. Lund, K. Rundqvist, E. Nilsson, L. Yu, B. Hagström and C. Müller, *npj Flex. Electron.*, 2018, **2**, 9.
30. N. Soin, T. H. Shah, S. C. Anand, J. F. Geng, W. Pornwannachai, P. Mandal, D. Reid, S. Sharma, R. L. Hadimani, D. V. Bayramol and E. Siores, *Energy Environ. Sci.*, 2014, **7**, 1670-1679.
31. E. Kabir, M. Khatun, L. Nasrin, M. J. Raihan and M. Rahman, *J. Phys. D: Appl. Phys*, 2017, **50**, 163002.
32. S. Bodkhe, G. Turcot, F. P. Gosselin and D. Therriault, *ACS Appl. Mater. Interfaces*, 2017, **9**, 20833-20842.
33. D. Singh, A. Choudhary and A. Garg, *ACS Appl. Mater. Interfaces*, 2018, **10**, 2793-2800.
34. A. S. Elniezayyen, F. M. Reicha, I. M. El-Sherbiny, J. M. Zheng and C. Y. Xu, *Eur. Polym. J.*, 2017, **90**, 195-208.
35. C. K. Jeong, C. Baek, A. I. Kingon, K. I. Park and S. H. Kim, *Small*, 2018, **14**, 8.
36. J. H. Lee, K. Y. Lee, B. Kumar, N. T. Tien, N. E. Lee and S. W. Kim, *Energy Environ. Sci.*, 2013, **6**, 169-175.
37. M. Y. Li, H. J. Wondergem, M.-J. Spijkman, K. Asadi, I. Katsouras, P. W. M. Blom and D. M. de Leeuw, *Nat. Mater.*, 2013, **12**, 433.
38. M. Y. Li, I. Katsouras, C. Piliego, G. Glasser, I. Lieberwirth, P. W. M. Blom and D. M. de Leeuw, *J. Mater. Chem. C*, 2013, **1**, 7695-7702.
39. A. C. Lopes, J. Gutierrez and J. M. Barandiaran, *Eur. Polym. J.*, 2018, **99**, 111-116.
40. C. Y. Xing, L. P. Zhao, J. C. You, W. Y. Dong, X. J. Cao and Y. J. Li, *J. Phys. Chem. B*, 2012, **116**, 8312-8320.
41. Measurement Specialities Inc, *Piezo Film Sensors, Technical Manual*, Sensor Products Division, USA, 1999.
42. Kureha Corporation, Piezo Films by Kureha, http://www.piezofilms.com, (accessed July, 2018).
43. P. Martins, A. C. Lopes and S. Lanceros-Mendez, *Prog. Polym. Sci.*, 2014, **39**, 683-706.
44. D. Damjanovic, in *The Science of Hysteresis*, eds. G. Bertotti and I. D. Mayergoyz, Academic Press, Oxford, 2006, DOI: 10.1016/B978-012480874-4/50022-1, pp. 337-465.
45. A. Vinogradov, in *Encyclopedia of smart materials*, ed. M. Schwartz, 2002, DOI: 10.1002/0471216275.esm061.
46. C. K. Lee, *J. Acoust. Soc. Am.*, 1990, **87**, 1144-1158.
47. H. F. Tiersten, *IEEE Trans. Ultrason. Ferroelectr. Freq. Control*, 1996, **43**, 717.
48. A. Erturk and D. J. Inman, in *Piezoelectric Energy Harvesting*, John Wiley & Sons, Ltd, 2011, DOI: 10.1002/9781119991151.app1, pp. 343-348.
49. Z. L. Wang, *Mater. Today*, 2017, **20**, 74-82.
50. G. G. Yaralioglu, A. S. Ergun, B. Bayram, E. Haeggstrom and B. T. Khuri-Yakub, *IEEE Trans. Ultrason. Ferroelectr. Freq. Control*, 2003, **50**, 449-456.
51. D. B. Deutz, J.-A. Pascoe, B. Schelen, S. van der Zwaag, D. M. de Leeuw and P. Groen, *Mater. Horizons*, 2018, **5**, 444-453.
52. M. Broadhurst, G. Davis, J. McKinney and R. Collins, *J. Appl. Phys*, 1978, **49**, 4992-4997.
53. Q. M. Zhang, V. Bharti and G. Kavarnos, in *Encyclopedia of Smart Materials*, ed. M. Schwartz, 2002, DOI: doi:10.1002/0471216275.esm063.
54. L. Ruan, X. Yao, Y. Chang, L. Zhou, G. Qin and X. Zhang, *Polymers*, 2018, **10**, 228.
55. J. Martin, D. Zhao, T. Lenz, I. Katsouras, D. M. de Leeuw and N. Stingelin, *Mater. Horizons*, 2017, **4**, 408-414.
56. V. Sencadas, S. Lanceros-Méndez and J. F. Mano, *Thermochim. Acta*, 2004, **424**, 201-207.
57. B. Ameduri, *Chem. Rev.*, 2009, **109**, 6632-6686.
58. P. Destruel, F. S. Rojas, D. Tougne and Hoang ‐ The ‐ Giam, *J. Appl. Phys*, 1984, **56**, 3298-3303.
59. J. Döring, V. Bovtun, J. Bartusch, U. Beck and M. Kreutzbruck, Cellular polypropylene ferroelectret film: Piezoelectric material for non-contact ultrasonic transducers, China, 2008.
60. S. Crossley, R. A. Whiter and S. Kar-Narayan, *Mater. Sci. Technol.*, 2014, **30**, 1613-1624.
61. C. Jean-Mistral, S. Basrour and J. J. Chaillout, *Smart Mater. Struct.*, 2010, **19**.
62. R. Calio, U. B. Rongala, D. Camboni, M. Milazzo, C. Stefanini, G. de Petris and C. M. Oddo, *Sensors*, 2014, **14**, 4755-4790.
63. C. Bowen, H. Kim, P. Weaver and S. Dunn, *Energy Environ. Sci.*, 2014, **7**, 25-44.
64. C. Y. Li, P. M. Wu, S. Lee, A. Gorton, M. J. Schulz and C. H. Ahn, *J. Microelectromech. Syst.*, 2008, **17**, 334-341.
65. K. Uchino, *Energy Technol.*, 2017, **6**, 829-848.
66. A. J. Lovinger, D. D. Davis, R. E. Cais and J. M. Kometani, *Macromolecules*, 1986, **19**, 1491-1494.
67. Y. Murata and N. Koizumi, *Polym. J.*, 1985, **17**, 1071.
68. S. Lanceros-Méndez, J. F. Mano, A. M. Costa and V. H. Schmidt, *J. Macromol. Sci., Part B: Phys.*, 2001, **40**, 517-527.
69. A. Vinogradov and F. Holloway, *Ferroelectrics*, 1999, **226**, 169-181.
70. F. R. Fan, W. Tang and Z. L. Wang, *Adv. Mater.*, 2016, **28**, 4283-4305.
71. C. Dagdeviren, B. D. Yang, Y. Su, P. L. Tran, P. Joe, E. Anderson, J. Xia, V. Doraiswamy, B. Dehdashti, X. Feng, B. Lu, R. Poston, Z. Khalpey, R. Ghaffari, Y. Huang, M. J. Slepian and J. A. Rogers, *Proceedings of the National Academy of Sciences*, 2014, **111**, 1927.
72. C. Dagdeviren, P. Joe, O. L. Tuzman, K.-I. Park, K. J. Lee, Y. Shi, Y. Huang and J. A. Rogers, *Extreme Mechanics Letters*, 2016, **9**, 269-281.
73. G.-T. Hwang, Y. Kim, J.-H. Lee, S. Oh, C. K. Jeong, D. Y. Park, J. Ryu, H. Kwon, S.-G. Lee, B. Joung, D. Kim and K. J. Lee, *Energy Environ. Sci.*, 2015, **8**, 2677-2684.
74. V. Cardoso, D. Correia, C. Ribeiro, M. Fernandes and S. Lanceros-Méndez, *Polymers*, 2018, **10**, 161.
75. C. Chandrana, J. Talman, T. Pan, S. Roy and A. Fleischman, *Sensors*, 2010, **10**, 8740.
76. M. A. Bachmann, W. L. Gordon, J. L. Koenig and J. B. Lando, *J. Appl. Phys*, 1979, **50**, 6106-6112.
77. W. M. Prest and D. J. Luca, *J. Appl. Phys*, 1978, **49**, 5042-5047.
78. M. T. Riosbaas, K. J. Loh, G. O'Bryan and B. R. Loyola, In Situ Phase Change Characterization of PVDF Thin Films using Raman Spectroscopy, USA, 2014.
79. W. J. Li, Q. J. Meng, Y. S. Zheng, Z. C. Zhang, W. M. Xia and Z. Xu, *Appl. Phys. Lett.*, 2010, **96**, 3.
80. K. Uchino, *Introduction to Piezoelectric Actuators and Transducers*, Pennsylvania State University, 2003.
81. A. Mohebbi and D. Rodrigue, *Polym. Eng. Sci.*, 2017, **58**, 300-309.
82. D. M. Esterly and B. J. Love, *J. Polym. Sci., Part B: Polym. Lett.*, 2004, **42**, 91-97.

83. R. Gregorio and M. Cestari, *J. Polym. Sci., Part B: Polym. Lett.*, 1994, **32**, 859-870.
84. B. S. Ince-Gunduz, K. Burke, M. Koplitz, M. Meleski, A. Sagiv and P. Cebe, *J. Macromol. Sci., Part A: Pure Appl.Chem.*, 2010, **47**, 1208-1219.
85. X. M. Cai, T. P. Lei, D. H. Sun and L. W. Lin, *RSC Adv.*, 2017, **7**, 15382-15389.
86. S. Barrau, A. Ferri, A. Da Costa, J. Defebvin, S. Leroy, R. Desfeux and J. M. Lefebvre, *ACS Appl. Mater. Interfaces*, 2018, **10**, 13092-13099.
87. H. Kim, T. Fernando, M. Y. Li, Y. R. Lin and T. L. B. Tseng, *J. Compos Mater.*, 2018, **52**, 197-206.
88. J. E. Lee and S. N. Leung, *CrystEngComm*, 2018, **20**, 11.
89. D. C. Bassett, *Developments in crystalline polymers*, Springer, 1982.
90. G. Teyssedre, A. Bernes and C. Lacabanne, *J. Polym. Sci., Part B: Polym. Lett.*, 1993, **31**, 2027-2034.
91. C. J. L. Constantino, A. E. Job, R. D. Simoes, J. A. Giacometti, V. Zucolotto, O. N. Oliveira, G. Gozzi and D. L. Chinaglia, *Appl. Spectrosc.*, 2005, **59**, 275-279.
92. C. J. L. Constantino, A. E. Job, R. D. Simoes, J. A. Giacometti, V. Zucolotto, O. N. Oliveira, G. Gozzi and D. L. Chinaglia, The investigation of alpha -> beta phase transition in poly(vinylidene fluoride) (PVDF), Brazil, 2005.
93. O. Garcia-Zaldivar, T. Escamilla-Diaz, M. Ramirez-Cardona, M. A. Hernandez-Landaverde, R. Ramirez-Bon, J. M. Yanez-Limon and F. Calderon-Pinar, *Sci. Rep.*, 2017, **7**.
94. S. K. Pradhan, A. Kumar, A. N. Sinha, P. Kour, R. Pandey, P. Kumar and M. Kar, *Ferroelectrics*, 2017, **516**, 18-27.
95. D. Sengupta, A. G. P. Kottapalli, S. H. Chen, J. M. Miao, C. Y. Kwok, M. S. Triantafyllou, M. E. Warkiani and M. Asadnia, *AIP Adv.*, 2017, **7**.
96. F. Xu, K. Zhang, Y. Zhou, Z. Qu, H. Wang, Y. Zhang, H. Zhou and C. Yan, *RSC Adv.*, 2017, **7**, 17038-17043.
97. M. H. Ghajar, M. M. Mashhadi, M. Irannejad, S. Jebril, M. Yavuz and E. Abdel-Rahman, *Polym. Compos.*, 2018, **39**, E1208-E1215.
98. M. H. Ghajar, M. M. Mashhadi, M. Irannejad, M. Yavuz and E. Abdel-Rahman, *Bull. Mater. Sci.*, 2018, **41**.
99. J. Ma, Q. Zhang, K. Lin, L. Zhou and Z. Ni, *Mater. Res. Express*, 2018, **5**.
100. S. Zhang, H. Wang, D. Xu, W. Yang, P. Tang and Y. Bin, *J. Appl. Polym. Sci.*, 2016, **133**.
101. V. Bhavanasi, V. Kumar, K. Parida, J. X. Wang and P. S. Lee, *ACS Appl. Mater. Interfaces*, 2016, **8**, 521-529.
102. J. Y. Lim, S. Kim and Y. Seo, Enhancement of beta-phase in PVDF by Electrospinning, USA, 2015.
103. M. Guerre, G. Lopez, T. Soulestin, C. Totee, B. Ameduri, G. Silly and V. Ladmiral, *Macromol. Chem. Phys.*, 2016, **217**, 2275-2285.
104. R. A. Ferren, in *The Applications of Ferroelectric Polymers*, eds. T. T. Wang, J. M. Herbert and A. M. Glass, Blackie & Son, Glasgow, 1988.
105. R. Timmerman and W. Greyson, *J. Appl. Polym. Sci.*, 1962, **6**, 456-460.
106. D. A. Seiler, in *Modern Fluoropolymers*, ed. J. E. Scheirs, Wiley, Chichester, UK, 1997, pp. 487-505.
107. T. Soulestin, V. Ladmiral, F. D. Dos Santos and B. Ameduri, *Prog. Polym. Sci.*, 2017, **72**, 16-60.
108. B. Ameduri, C. Ladavière, F. Delolme and B. Boutevin, *Macromolecules*, 2004, **37**, 7602-7609.
109. R. E. Cais and J. M. Kometani, *Macromolecules*, 1985, **18**, 1354-1357.
110. A. J. Lovinger, D. D. Davis, R. E. Cais and J. M. Kometani, *Polymer*, 1987, **28**, 617-626.
111. T. S. Wang, M. Farajollahi, Y. S. Choi, I. T. Lin, J. E. Marshall, N. M. Thompson, S. Kar-Narayan, J. D. W. Madden and S. K. Smoukov, *Interface Focus*, 2016, **6**, 19.
112. Z. Li, J. Wang, X. Wang, Q. H. Yang and Z. C. Zhang, *RSC Adv.*, 2015, **5**, 80950-80955.
113. E. Klimiec, W. Zaraska, K. Zaraska, A. Cichocki, K. Gąsiorwski, T. Sadowski and M. Pajda, *Elektronika: konstrukcje, technologie, zastosowania*, 2006, **47**, 11-13.
114. F. Wang, P. Frubing, W. Wirges, R. Gerhard and M. Wegener, *IEEE Trans. Dielectr. Electr. Insul.*, 2010, **17**, 1088-1095.
115. Y. Wang, B. Neese, Q. M. Zhang, C. Huang and J. West, High Piezoelectric Responses in P(VDF HFP) Copolymers for Sensors and Transducers, USA, 2007.
116. Z. Li, Y. Wang and Z.-Y. Cheng, *Appl. Phys. Lett.*, 2006, **88**, 062904.
117. T. Yagi and M. Tatemoto, *Polym. J.*, 1979, **11**, 429.
118. A. J. Lovinger, *Science*, 1983, **220**, 1115.
119. E. Fukada, *IEEE Trans. Ultrason. Ferroelectr. Freq. Control*, 2000, **47**, 1277-1290.
120. T. Furukawa, *Phase Transit.*, 1989, **18**, 143-211.
121. K. Tashiro, H. Tadokoro and M. Kobayashi, *Ferroelectrics*, 1981, **32**, 167-175.
122. B. Neese, Y. Wang, B. Chu, K. Ren, S. Liu, Q. M. Zhang, C. Huang and J. West, *Appl. Phys. Lett.*, 2007, **90**, 242917.
123. B. Hu, N. Hu, L. K. Wu, F. Liu, Y. L. Liu, H. M. Ning, S. Atobe and H. Fukunaga, *J. Polym. Eng.*, 2015, **35**, 451-461.
124. R. E. Sousa, J. Nunes-Pereira, J. C. C. Ferreira, C. M. Costa, A. V. Machado, M. M. Silva and S. Lanceros-Mendez, *Polym. Test*, 2014, **40**, 245-255.
125. B. Améduri, B. Boutevin and G. Kostov, *Prog. Polym. Sci.*, 2001, **26**, 105-187.
126. T. S. Ahmed, J. M. DeSimone and G. W. Roberts, *Macromolecules*, 2007, **40**, 9322-9331.
127. L. Xiaoyan, A. Schirokauer and J. Scheinbeim, *IEEE Trans. Ultrason. Ferroelectr. Freq. Control*, 2000, **47**, 1291-1295.
128. P. Sukwisute, N. Muensit, S. Soontaranon and S. Rugmai, *Appl. Phys. Lett.*, 2013, **103**, 063905.
129. N. K. Kalfoglou and H. L. Williams, *J. Appl. Polym. Sci.*, 1973, **17**, 3367-3373.
130. M. Latour and H. A. Dorra, *Ferroelectrics*, 1982, **44**, 197-203.
131. T. Hattori, M. Hikosaka and H. Ohigashi, *Polymer*, 1996, **37**, 85-91.
132. D. Yang and Y. Chen, *J. Mater. Sci. Lett.*, 1987, **6**, 599-603.
133. J. P. Luongo, *J. Polym. Sci., Part A: Gen. Pap.*, 1972, **10**, 1119-1123.
134. H. Kawai, *Jpn. J. Appl. Phys.*, 1969, **8**, 975.
135. W. W. Doll and J. B. Lando, *J. Macromol. Sci., Part B: Phys.*, 1970, **4**, 309-329.
136. W. W. Doll and J. B. Lando, *J. Macromol. Sci., Part B: Phys.*, 1970, **4**, 889-896.
137. J. Scheinbeim, C. Nakafuku, B. A. Newman and K. D. Pae, *J. Appl. Phys*, 1979, **50**, 4399-4405.
138. M. M. D. Ramos, H. M. G. Correia and S. Lanceros-Méndez, *Comput. Mater. Sci.*, 2005, **33**, 230-236.
139. S. Ramasundaram, S. Yoon, K. J. Kim and J. S. Lee, *Macromol. Chem. Phys.*, 2008, **209**, 2516-2526.

140. S. Chen, X. Li, K. Yao, F. E. H. Tay, A. Kumar and K. Zeng, *Polymer*, 2012, **53**, 1404-1408.
141. J. R. Gregorio and C. Marcelo, *J. Polym. Sci., Part B: Polym. Lett.*, 1994, **32**, 859-870.
142. M. Benz, W. B. Euler and O. J. Gregory, *Macromolecules*, 2002, **35**, 2682-2688.
143. J. Nunes-Pereira, P. Martins, V. F. Cardoso, C. M. Costa and S. Lanceros-Mendez, *Mater. Des.*, 2016, **104**, 183-189.
144. M. S. S. and T. A. H., *Chem. Eng. Technol.*, 2011, **34**, 1328-1334.
145. Z.-M. Huang, Y. Z. Zhang, M. Kotaki and S. Ramakrishna, *Compos. Sci. Technol.*, 2003, **63**, 2223-2253.
146. C. Ribeiro, V. Sencadas, J. L. G. Ribelles and S. Lanceros-Méndez, *Soft Mater.*, 2010, **8**, 274-287.
147. C. Ribeiro, D. M. Correia, S. Ribeiro, V. Sencadas, G. Botelho and S. Lanceros-Mendez, *Eng. Life Sci.*, 2015, **15**, 351-356.
148. L. Persano, A. Camposeo, C. Tekmen and D. Pisignano, *Macromol. Mater. Eng.*, 2013, **298**, 504-520.
149. F. Mokhtari, M. Latifi and M. Shamshirsaz, *J. Text. Inst.*, 2016, **107**, 1037-1055.
150. H. Shao, J. Fang, H. Wang and T. Lin, *RSC Adv.*, 2015, **5**, 14345-14350.
151. Y. Bin, Y. Hao, M. Mengye, W. Hongzhi and Z. Meifang, Enhanced output power polyvinylidene fluoride (PVDF) electrospun nanogenerator with high fiber alignment, Italy, 2015.
152. P. Hu, D. Zheng, C. Zhao, Y. Zhang and J. Niu, *Mater. Lett.*, 2018, **218**, 71-75.
153. G. Roberts, *Langmuir-blodgett films*, Springer Science & Business Media, 2013.
154. H. Zhu, S. Yamamoto, J. Matsui, T. Miyashita and M. Mitsuishi, *RSC Adv.*, 2016, **6**, 32007-32012.
155. H. Zhu, M. Mitsuishi and T. Miyashita, *Macromolecules*, 2012, **45**, 9076-9084.
156. Y. Jiang, Y. U. N. Ye, J. Yu, Y. Yang, J. Xu and Z. Wu, *Integr. Ferroelectr.*, 2007, **88**, 21-26.
157. Z. Huie, G. Yu, Y. Shunsuke, M. Tokuji and M. Masaya, *Jpn. J. Appl. Phys.*, 2016, **55**, 03DD11.
158. W. Y. Kim, D. Song, G. Jeon, I. K. Kang, H. B. Shim, D. Kim, H. C. Lee, H. Park, S. Kang and J. Bae, *Micro Nano Lett.*, 2015, **10**, 384-388.
159. Y. Y. Choi, P. Sharma, C. Phatak, D. J. Gosztola, Y. Y. Liu, J. Lee, B. Lee, J. Y. Li, A. Gruverman, S. Ducharme and S. Hong, *ACS Nano*, 2015, **9**, 1809-1819.
160. E. V. Paramonova, S. V. Filippov, V. E. Gevorkyan, L. A. Avakyan, X. J. Meng, B. B. Tian, J. L. Wang and V. S. Bystrov, *Ferroelectrics*, 2017, **509**, 143-157.
161. H. Zhu, S. Yamamoto, J. Matsui, T. Miyashita and M. Mitsuishi, *RSC Adv.*, 2018, **8**, 7963-7968.
162. Tecdia Inc, *ARQUE catalog*, Campbell, USA, 2017.
163. K. Kim, W. Zhu, X. Qu, C. Aaronson, W. R. McCall, S. Chen and D. J. Sirbuly, *ACS Nano*, 2014, **8**, 9799-9806.
164. H. Kim, F. Torres, Y. Wu, D. Villagran, Y. Lin and T.-L. Tseng, *Smart Mater. Struct.*, 2017, **26**, 085027.
165. C. Lee and J. A. Tarbutton, *Smart Mater. Struct.*, 2014, **23**, 7.
166. J. H. Yang, T. Ryu, Y. Lansac, Y. H. Jang and B. H. Lee, *Org. Electron.*, 2016, **28**, 67-72.
167. J. Oliveira, V. Correia, H. Castro, P. Martins and S. Lanceros-Mendez, *Additive Manufact.*, 2018, **21**, 269-283.
168. S. Bodkhe, P. S. M. Rajesh, F. P. Gosselin and D. Therriault, *ACS Appl. Energy Mater.*, 2018, **1**, 2474-2482.
169. S. Bodkhe, C. Noonan, F. P. Gosselin and D. Therriault, *Adv. Eng. Mater.*, DOI: 10.1002/adem.201800206.
170. A. H. Rajabi, M. Jaffe and T. L. Arinzeh, *Acta Biomater.*, 2015, **24**, 12-23.
171. C. Park, Z. Ounaies, K. E. Wise and J. S. Harrison, *Polymer*, 2004, **45**, 5417-5425.
172. C. Li, P. M. Wu, S. Lee, A. Gorton, M. J. Schulz and C. H. Ahn, *J. Microelectromech. Syst.*, 2008, **17**, 334-341.
173. S. K. Mahadeva, J. Berring, K. Walus and B. Stoeber, *J. Phys. D: Appl. Phys*, 2013, **46**, 7.
174. B. Gross, R. Gerhard‐Multhaupt, A. Berraissoul and G. M. Sessler, *J. Appl. Phys*, 1987, **62**, 1429-1432.
175. R. Gerhard, in *Electromechanically Active Polymers: A Concise Reference*, ed. F. Carpi, Springer International Publishing, Cham, 2016, pp. 1-19.
176. P.-H. Ducrot, I. Dufour and C. Ayela, *Sci. Rep.*, 2016, **6**, 19426.
177. S. Rajala, M. Schouten, G. Krijnen and S. Tuukkanen, *ACS Omega*, 2018, **3**, 8067-8073.
178. S. K. Ghosh, A. Biswas, S. Sen, C. Das, K. Henkel, D. Schmeissere and D. Mandal, *Nano Energy*, 2016, **30**, 621-629.
179. P. Thakur, A. Kool, N. A. Hoque, B. Bagchi, F. Khatun, P. Biswas, D. Brahma, S. Roy, S. Banerjee and S. Das, *Nano Energy*, 2018, **44**, 456-467.
180. K. Maity and D. Mandal, *AIP Conf. Proc.*, 2018, **1942**, 050088.
181. M. Pusty, A. Sharma, L. Sinha, A. Chaudhary and P. Shirage, *ChemistrySelect*, 2017, **2**, 2774-2782.
182. S. K. Karan, R. Bera, S. Paria, A. K. Das, S. Maiti, A. Maitra and B. B. Khatua, *Adv. Energy Mater.*, 2016, **6**, 1601016.
183. R. A. Whiter, V. Narayan and S. Kar-Narayan, *Adv. Energy Mater.*, 2014, **4**, 1400519.
184. A. Tamang, S. K. Ghosh, S. Garain, M. M. Alam, J. Haeberle, K. Henkel, D. Schmeisser and D. Mandal, *ACS Appl. Mater. Interfaces*, 2015, **7**, 16143-16147.
185. H. J. Ye, W. Z. Shao and L. Zhen, *J. Appl. Polym. Sci.*, 2013, **129**, 2940-2949.
186. S. F. Mendes, C. M. Costa, C. Caparros, V. Sencadas and S. Lanceros-Méndez, *J. Mater. Sci.*, 2012, **47**, 1378-1388.
187. M. Sharma, J. K. Quamara and A. Gaur, *J. Mater. Sci. Mater. Electron.*, 2018, **29**, 10875-10884.
188. P. Martins, C. M. Costa and S. Lanceros-Mendez, *Appl. Phys. A Mater. Sci. Process.*, 2011, **103**, 233-237.
189. L. M. Saleh Medina and R. M. Negri, *J. Phys. Chem. C*, 2017, **121**, 27683-27692.
190. M. S. Sebastian, A. Larrea, R. Gonçalves, T. Alejo, J. L. Vilas, V. Sebastian, P. Martins and S. Lanceros-Mendez, *RSC Adv.*, 2016, **6**, 113007-113015.
191. A. Samadi, S. M. Hosseini and M. Mohseni, *Org. Electron.*, 2018, **59**, 149-155.
192. N. An, H. Liu, Y. Ding, M. Zhang and Y. Tang, *Appl. Surf. Sci.*, 2011, **257**, 3831-3835.
193. D. Mandal, K. J. Kim and J. S. Lee, *Langmuir*, 2012, **28**, 10310-10317.
194. W. Wang, S. Zhang, L. o. Srisombat, T. R. Lee and R. C. Advincula, *Macromol. Mater. Eng.*, 2011, **296**, 178-184.
195. S. Yu, W. Zheng, W. Yu, Y. Zhang, Q. Jiang and Z. Zhao, *Macromolecules*, 2009, **42**, 8870-8874.
196. C. Xing, L. Zhao, J. You, W. Dong, X. Cao and Y. Li, *J. Phys. Chem. B*, 2012, **116**, 8312-8320.

197. N. Maity, A. Mandal and A. K. Nandi, *Polymer*, 2015, **65**, 154-167.
198. J. C. Dias, A. C. Lopes, B. Magalhaes, G. Botelho, M. M. Silva, J. Esperanca and S. Lanceros-Mendez, *Polym. Test*, 2015, **48**, 199-205.
199. J. C. Dias, D. C. Correia, A. C. Lopes, S. Ribeiro, C. Ribeiro, V. Sencadas, G. Botelho, J. M. S. S. Esperança, J. M. Laza, J. L. Vilas, L. M. León and S. Lanceros-Méndez, *J. Mater. Sci.*, 2016, **51**, 4442-4450.
200. M. Fukagawa, Y. Koshiba, T. Fukushima, M. Morimoto and K. Ishida, *Jpn. J. Appl. Phys.*, 2018, **57**, 6.
201. V. K. Tiwari, Y. Lee, G. Song, K. Lib Kim, Y. Jung Park and C. Park, *J. Polym. Sci., Part B: Polym. Lett.*, 2018, **56**, 795-802.
202. Y. Zhu, C. Li, B. Na, R. Lv, B. Chen and J. Zhu, *Mater. Chem. Phys.*, 2014, **144**, 194-198.
203. J. Kymissis, C. Kendall, J. Paradiso and N. Gershenfeld, Parasitic power harvesting in shoes, USA, 1998.
204. S. Singh, V. K. Gupta and S. Mukherjee, *Mater. Phys. Mech.*, 2018, **37**, 159-167.
205. E. Klimiec, K. Zaraska, W. Zaraska and S. Kuczynski, Micropower Generators and Sensors Based On Piezoelectric Polypropylene PP and Polyvinylidene Fluoride PVDF Films - Energy Harvesting From Walking, Switzerland, 2012.
206. J. J. Zhao and Z. You, *Sensors*, 2014, **14**, 12497-12510.
207. Y. Cha, *J. Intell. Mater. Syst. Struct.*, 2017, **28**, 3006-3015.
208. Y. Xin, X. Li, H. Y. Tian, C. Guo, C. H. Qian, S. H. Wang and C. Wang, *Ferroelectrics*, 2016, **493**, 12-24.
209. J. Granstrom, J. Feenstra, H. A. Sodano and K. Farinholt, *Smart Mater. Struct.*, 2007, **16**, 1810-1820.
210. A. Gheibi, M. Latifi, A. A. Merati and R. Bagherzadeh, *J. Polym. Res.*, 2014, **21**, 7.
211. H. J. Sim, C. Choi, C. J. Lee, Y. T. Kim and S. J. Kim, *Curr. Nanosci.*, 2015, **11**, 539-544.
212. J. H. Yang, H. S. Cho, S. H. Park, S. H. Song, K. S. Yun and J. H. Lee, *Smart Mater. Struct.*, 2016, **25**, 15.
213. B. Z. Li, F. F. Zhang, S. Guan, J. M. Zheng and C. Y. Xu, *J. Mater. Chem. C*, 2016, **4**, 6988-6995.
214. A. Atalay, O. Atalay, M. D. Husain, A. Fernando and P. Potluri, *J. Ind. Text.*, 2017, **47**, 505-521.
215. R. L. Hadimani, D. V. Bayramol, N. Sion, T. Shah, L. M. Qian, S. X. Shi and E. Siores, *Smart Mater. Struct.*, 2013, **22**, 6.
216. K. Magniez, A. Krajewski, M. Neuenhofer and R. Helmer, *J. Appl. Polym. Sci.*, 2013, **129**, 2699-2706.
217. A. S. Krajewski, K. Magniez, R. J. N. Helmer and V. Schrank, *IEEE Sens. J.*, 2013, **13**, 4743-4748.
218. A. Talbourdet, F. Rault, G. Lemort, C. Cochrane, E. Devaux and C. Campagne, *Smart Mater. Struct.*, 2018, **27**, 7.
219. H. Gao, P. T. Minh, H. Wang, S. Minko, J. Locklin, T. Nguyen and S. Sharma, *Smart Mater. Struct.*, 2018, **27**, 11.
220. L. Engel, K. R. Van Volkinburg, M. Ben-David, G. N. Washington, S. Krylov and Y. Shacham-Diamand, Fabrication of a self-sensing electroactive polymer bimorph actuator based on polyvinylidene fluoride and its electrostrictive terpolymer, USA, 2016.
221. C. Lee, D. Wood, D. Edmondson, D. Y. Yao, A. E. Erickson, C. T. Tsao, R. A. Revia, H. Kim and M. Q. Zhang, *Ceram. Int.*, 2016, **42**, 2734-2740.
222. Z. Y. Zhang, C. H. Yao, Y. H. Yu, Z. L. Hong, M. J. Zhi and X. D. Wang, *Adv. Funct. Mater.*, 2016, **26**, 6760-6765.
223. J. W. Tsai, J. J. Wang, Y. C. Su and Ieee, Piezoelectric Rubber Films For Human Physiological Monitoring And Energy Harvesting, Taiwan, 2013.
224. D. H. Kim, H. J. Shin, H. Lee, C. K. Jeong, H. Park, G.-T. Hwang, H.-Y. Lee, D. J. Joe, J. H. Han, S. H. Lee, J. Kim, B. Joung and K. J. Lee, *Adv. Funct. Mater.*, 2017, **27**, 1700341.
225. E. Hausler, L. Stein and G. Harbauer, *Ferroelectrics*, 1984, **60**, 277-282.
226. X. L. Cheng, X. Xue, Y. Ma, M. D. Han, W. Zhang, Z. Y. Xu, H. Zhang and H. X. Zhang, *Nano Energy*, 2016, **22**, 453-460.
227. Y. H. Yu, H. Y. Sun, H. Orbay, F. Chen, C. G. England, W. B. Cai and X. D. Wang, *Nano Energy*, 2016, **27**, 275-281.
228. J. Li, L. Kang, Y. H. Yu, Y. Long, J. J. Jeffery, W. B. Cai and X. D. Wang, *Nano Energy*, 2018, **51**, 728-735.
229. J. H. Ahn, W. S. Hwang, J. Y. Cho, S. Y. Jeong, G. J. Song, S. D. Hong, T. H. Sung, S. Jeong and H. H. Yoo, *J. Korean Phys. Soc.*, 2018, **73**, 330-337.
230. Y. Song, C. H. Yang, S. K. Hong, S. J. Hwang, J. H. Kim, J. Y. Choi, S. K. Ryu and T. H. Sung, *Int. J. Hydrog. Energy*, 2016, **41**, 12563-12568.
231. R. Abinaya, V. Varsha and K. Hariharan, An intelligent street light system based on piezoelectric sensor networks, India, 2017.
232. C. H. Yang, Y. Song, M. S. Woo, J. H. Eom, G. J. Song, J. H. Kim, J. Kim, T. H. Lee, J. Y. Choi and T. H. Sung, *Sens. Actuators, A*, 2017, **261**, 317-324.
233. *US Pat.*, US7830071B2, 2010.
234. Y. Wang, X. Zhu, T. Zhang, S. Bano, H. Pan, L. Qi, Z. Zhang and Y. Yuan, *Appl. Energy*, 2018, **230**, 52-61.
235. D. Vatansever, R. L. Hadimani, T. Shah and E. Siores, *Smart Mater. Struct.*, 2011, **20**, 6.
236. S. G. Li and H. Lipson, Vertical-stalk flapping-leaf generator for wind energy harvesting, USA, 2009.
237. S. G. Li, J. P. Yuan and H. Lipson, *J. Appl. Phys*, 2011, **109**, 3.
238. D. J. Li, S. Hong, S. Y. Gu, Y. Choi, S. Nakhmanson, O. Heinonen, D. Karpeev and K. No, *Appl. Phys. Lett.*, 2014, **104**, 4.
239. J. D. Song, G. X. Zhao, B. Li and J. Wang, *Heliyon*, 2017, **3**, 18.